Available online at www.sciencedirect.com

SciVerse ScienceDirect

Geochimica et Cosmochimica Acta 75 (2011) 6374–6399

Geochimica et Cosmochimica Acta

www.elsevier.com/locate/gca

Improved provenance tracing of Asian dust sources using rare earth elements and selected trace elements for palaeomonsoon studies on the eastern Tibetan Plateau

Marion Ferrat [a,*], Dominik J. Weiss [a,b], Stanislav Strekopytov [b], Shuofei Dong [a], Hongyun Chen [c], Jens Najorka [b], Youbin Sun [c], Sanjeev Gupta [a], Ryuji Tada [d], Rajiv Sinha [e]

[a] *Department of Earth Sciences and Engineering, Imperial College London, London SW7 2BP, UK*
[b] *Department of Mineralogy, The Natural History Museum, Cromwell Road, London SW7 5BD, UK*
[c] *State Key Laboratory of Loess and Quaternary Geology, Institute of Earth Environment, Chinese Academy of Sciences, Xi'An 710075, China*
[d] *Department of Earth and Planetary Science, University of Tokyo, Tokyo, Japan*
[e] *Department of Civil Engineering, Indian Institute of Technology, Kanpur 208016, Uttar Pradesh, India*

Received 22 February 2011; accepted in revised form 5 August 2011; available online 26 August 2011

Abstract

The Asian Monsoon forms an important part of the earth's climate system, yet our understanding of the past interactions between its different sub-systems, the East Asian and Indian monsoons, and between monsoonal winds and other prevailing wind currents such as the Westerly jet, is limited, particularly in central Asia. This in turn affects our ability to develop climate models capable of accurately predicting future changes in atmospheric circulation patterns and monsoon intensities in Asia. Provenance studies of mineral dust deposited in terrestrial settings such as peat bogs can address this problem directly, by offering the possibility to examine past deposition rates and wind direction, and hence reconstruct past atmospheric circulation patterns. However, such studies are challenged by several issues, most importantly the identification of proxies that unambiguously distinguish between the different potential dust sources and that are independent of particle size. In addition, a single analytical method that is suitable for sample preparation of both dust source (i.e. desert sand, soil) and receptor (i.e. dust archive such as peat or soil profiles) material is desirable in order to minimize error propagation derived from the experimental and analytical work. Here, an improved geochemical framework of provenance tracers to study atmospheric circulation patterns and palaeomonsoon variability in central Asia is provided, by combining for the first time mineralogical as well as major and trace elemental (Sc, Y, Th and the rare earth elements) information on Chinese (central Chinese loess plateau, northern Qaidam basin and Taklamakan, Badain Juran and Tengger deserts), Indian (Thar desert) and Tibetan (eastern Qinghai–Tibetan Plateau) dust sources.

Quartz, feldspars and clay minerals are the major constituents of all studied sources, with highly variable calcite contents reflected in the CaO concentrations. Chinese and Tibetan dust sources are enriched in middle REE relative to the upper continental crust and average shale but the Thar desert has a REE signature distinctly different from all other dust sources. There are significant differences in major, trace and REE compositions between the coarse and fine fractions of the surface sands, with the finest <4 μm fraction enriched in Al_2O_3, Fe_2O_3, MnO, MgO and K_2O and the <32 μm fractions in Sc, Y, Th and the REE relative to the coarse fractions. The <4 μm fraction best represents the bulk REE geochemistry of the samples. The provenance tracers Y/∑REE, La/Er, La/Gd, Gd/Er, La/Yb, Y/Tb, Y/La, Y/Nd and to a certain extent the europium anomaly Eu/Eu* (all REE normalized to post-Archean Australian shale, PAAS) are particle size-independent tracers, of which

* Corresponding author. Tel.: +44 7809614357.
E-mail address: marion.ferrat03@imperial.ac.uk (M. Ferrat).

doi:10.1016/j.gca.2011.08.025

combinations of Y/∑REE, La/Yb, Y/Tb, Y/La and Eu/Eu* can be used to distinguish the Thar desert, the Chinese deserts, the Chinese loess plateau and the Tibetan soils. Their independence upon grain size means that these tracers can be applied to the long-range provenance tracing of Asian dust even when only bulk samples are available in the source region. Combinations of La/Th, Y/Tb, Y/∑REE, Sc/La and Y/Er distinguish the Tibetan soils from the Chinese loess plateau and the Chinese deserts. La/Th and notably Th/∑REE isolate the signature of the Badain Juran desert and the combination of Sc/La and Y/Er that of the Taklamakan desert. The similarity in all trace and REE-based provenance tracers between the northern Qaidam basin and Tengger desert suggests that these two deposits may have a common aeolian source.

1. INTRODUCTION

The Holocene evolution of the East Asian and Indian monsoon systems has been reconstructed using high-resolution speleothem records from eastern China and Oman (Neff et al., 2001; Fleitmann et al., 2003; Dykoski et al., 2005; Wang et al., 2005a; Maher, 2008). The existing data indicate that the strength and dynamics of the monsoonal circulation are significantly correlated with orbital forcing and the resulting changes in northern hemisphere solar insolation. However, continental sites at the marginal zones of the monsoon influence, such as lake sediments and loess–paleosol sequences in northern central China, reveal significant spatial and temporal winter and summer monsoon variability during the Holocene (An et al., 2000; Stevens et al., 2007; Chen et al., 2008; Maher, 2008). A comprehensive discussion of the possible reasons for the mismatch between the in-phase changes recorded in the coastal cave deposits, and out-of-phase changes in central Asia, is hampered by the scarcity of terrestrial records in this region (Wang et al., 2005b; Maher, 2008; Liu et al., 2009).

One approach to constrain past atmospheric circulation in central Asia is the study of wind direction and wind strength derived from terrestrial archives of mineral dust deposition (e.g. Svensson et al., 2000; Ding et al., 2001; Chen et al., 2006). Mineral dust particles emitted from arid regions, transported in the atmosphere and deposited in terrestrial settings such as peatlands, make up records which offer the potential to elucidate changes in past circulation patterns (e.g. Kylander et al., 2007). The eastern Qinghai–Tibetan Plateau is a region of particular relevance to dust provenance studies as it is under the influence of a variety of wind currents, including the East Asian winter and summer monsoons, the Indian summer monsoon and the Westerly jet (Fig. 1). The determination of the origin of mineral dust deposited at a site can provide means to interpret which wind system was dominant at that particular location through time and interpret changes in atmospheric circulation patterns. In order to understand which deserts contributed to past dust deposition on the eastern Tibetan Plateau, specific dust provenance tracers unique to each potential dust source must be identified.

Selected trace elements such as the rare earth elements (REE), Y, Sc and Th have been widely applied to provenance studies of atmospheric dust (Gallet et al., 1996, 1998; Jahn et al., 2001; Pease and Tchakerian, 2002; Zdanowicz et al., 2006). However, source specific trace element-based provenance tracers for Chinese, Tibetan and Indian dust sources remain limited, precluding the accurate study of palaeomonsoon evolution in central Asia. In order to identify such tracers, several considerations must be taken into account.

First, the geochemical composition of the deposited dust and its potential sources must be determined, ideally via a single reliable dissolution method. This minimizes analytical inaccuracies when comparing samples of different origin and ensures that a direct comparison of their compositions is valid. Second, the effect of particle size on individual dust provenance tracers must be investigated. The major and trace element (REE, Sc, Y and Th) composition of dust particles is found to vary with particle size both in Asian desert sands (Chang et al., 2000; Honda et al., 2004; Yang et al., 2007a,b; Xiong et al., 2010) and suspended aerosols (Kanayama et al., 2005), making it important to compare the relevant fraction in the source region which was effectively deposited in the archive. For example, while long-range dust particles to Greenland or North America are generally found to have diameters <5 μm (Steffensen, 1997; Zdanowicz et al., 2006), coarser dust particles with diameters <16 μm may be transported over China and Japan (Zhang et al., 2003a,b; Sun et al., 2007; Wu et al., 2009a) and Asian dust particles with diameters exceeding 10 μm have been recovered as far as a high altitude ice core in Canada (Zdanowicz et al., 2006). The selection of the relevant size fraction in the source regions is thus paramount to the correct comparison between the deposited dust and its potential source(s). In this context, of specific interest is the establishment of provenance tracers independent of grain size. Third, an exhaustive comparison of trace and REE-based proxies must be carried out and a multi-proxy database of source specific provenance tracers for Chinese, Indian and Tibetan dust sources must be determined. Elemental ratios are more representative than individual concentrations in the distinction between aeolian dust sources as they omit dilution effects of certain minerals and allow the combination of different trends in rare earth element and trace element patterns. The combination of REE and trace elements in proxy ratios for provenance tracing of Asian dust must be further explored to optimize the detection of compositional differences between the various sources.

These considerations have never, to the authors' knowledge, been addressed in a single study. Following from this, the aim of this work is to provide a reliable geochemical framework of provenance tracers allowing the identification of different Asian dust sources for the study of past dust transport to the eastern Tibetan Plateau and for reconstructions of past atmospheric circulation patterns in this region.

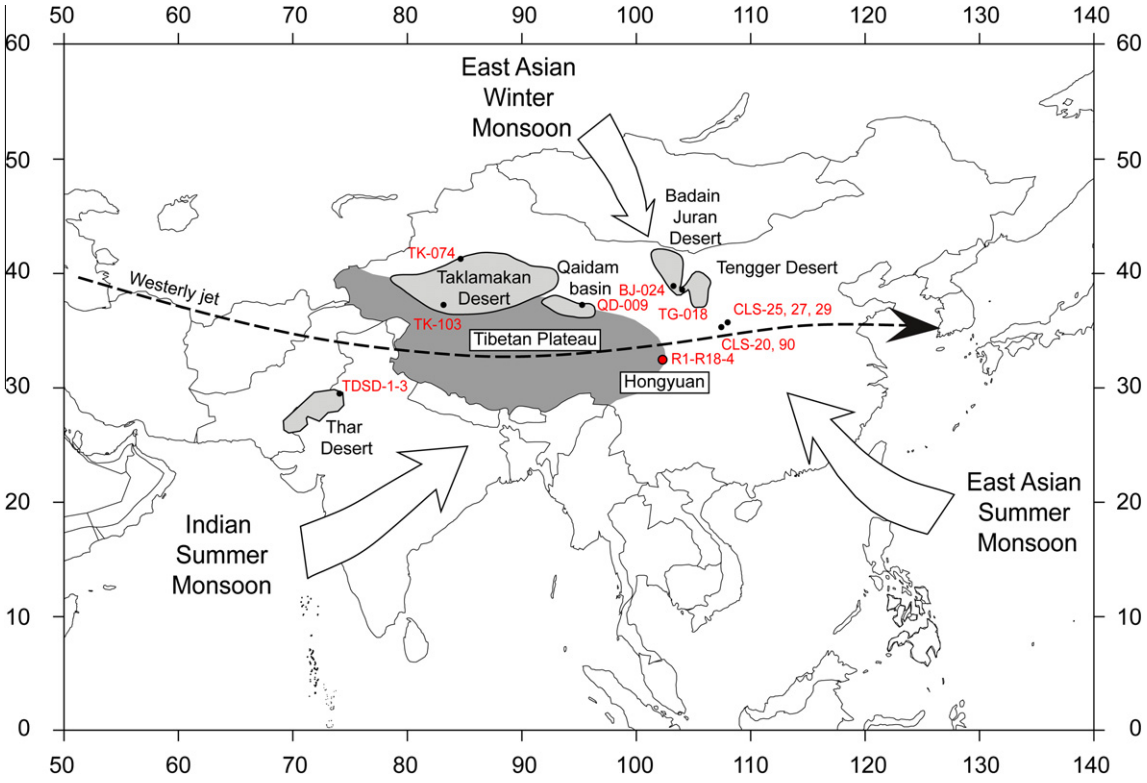

Fig. 1. Map showing the approximate location and sampling sites of the Asian dust sources considered in this study: the Taklamakan desert (samples TK-074 and TK-103) and Qaidam basin (QD-009) of northwestern China, the Tengger desert (TG-018), Badain Juran desert (BJ-024), and Chinese loess plateau (CLS-20-90) of northern China, the eastern Tibetan soils (R1–R18-4) and the Thar desert of northwestern India (TDSD 1-3). Arrows indicate the approximate wind directions associated with the East Asian summer and winter monsoons, the Indian summer monsoon and the Westerly jet. The location of the Hongyuan peat archive to which the provenance tracers will be applied in a following study is also shown.

Specifically, the objectives of this study are to: (i) determine the major and trace element composition of bulk and size separated surface samples from different Asian dust sources using a dissolution method applicable to a range of possible matrices; (ii) carry out a systematic and comparative investigation of the mineralogy and major and trace element (Sc, Y, Th and the REE) geochemistry of surface sands from six desert and loess deposits in China and India, as well as surface soils from the eastern Qinghai–Tibetan Plateau. We place a particular emphasis on the comparison of our results with previously published studies to determine which characteristics of the deposits are systematically observed; (iii) investigate the effect of grain size on the trace element composition of Chinese desert sands and determine particle size-independent proxies for the study of Asian dust transported to the eastern Qinghai–Tibetan Plateau; and (iv) identify the most reliable set of geochemical proxies to distinguish between these sources. In particular, provenance tracers are sought which would allow: (a) the distinction between Chinese versus Indian dust input, as this will have implications for the determination of the dominant hemispheric wind currents affecting this region and (b) the distinction between different Chinese dust sources (e.g. northwestern versus northern deserts, Chinese loess plateau), as this will allow the study of regional wind currents such as the northerly winter monsoon or the Westerly jet. These provenance tracers can be measured in mineral dust deposited in any terrestrial archive in this region for the study of past atmospheric circulation patterns and palaeomonsoon dynamics.

2. MATERIALS AND METHODS

2.1. Regional setting and sampling of the Asian dust sources

Surface samples from five Asian deserts, one section of the Chinese loess plateau and soils from the Qinghai–Tibetan Plateau were studied. The sampled deserts include the Taklamakan desert and Qaidam basin of northwestern China, the Badain Juran and Tengger deserts of northern China and the Thar desert of India (Fig. 1).

The Taklamakan desert in the Tarim basin covers an area of 337,000 km^2 and is thought to be the most active Asian emitter of long-range dust (Prospero et al., 2002). It is surrounded by the high Tianshan and Kunlun mountain ranges, which provide large quantities of detrital material to the basin (Honda and Shimizu, 1998; Chang et al., 2000). This desert is the main provider of dust to Greenland today (Bory et al., 2003) and possibly also was throughout the last glacial cycle (Svensson et al., 2000). It accounted, with the Gobi desert in southern Mongolia and sandy deserts in northern China, for 70% of the total modelled

Asian dust emissions between 1960 and 2000 (Zhang et al., 2003c).

The Badain Juran and Tengger deserts are bound by the Hexi corridor and Qilian mountains to the southwest. The Badain Juran desert is thought to be an important source of dust aerosols to Beijing during the dust storm season in spring (Yang et al., 2007a) and the Tengger desert that of dustfall events in Japan (Kanayama et al., 2002). Both deserts have been linked to recent dust events in the western United States (Husar et al., 2001) and the latter has also been considered a likely candidate for dust transport to Greenland outside of the high dust season (Bory et al., 2003).

The Qaidam basin, on the northeastern fringe of the Qinghai–Tibetan Plateau, has not of yet been shown to be an important emitter of long-range dust but frequent dust storms in spring have been identified as the possible primary source of material to the western Chinese loess plateau (Wu et al., 2009a). Dust emissions from the Chinese loess plateau itself are thought to be rather limited compared to the deserts in northern and northwestern China (Sun et al., 2001; Zhang et al., 2003c) but it has recently been found to be one of the potential sources of dust to Korea today (Lee et al., 2010).

In India, the Thar desert is a significant source of dust aerosols over South Asia (Yadav and Rajamani, 2004) and to the southern Himalayas (Carrico et al., 2003; Kang et al., 2004; Zhang et al., 2009). To our knowledge, very little geochemical data is available for this dust source and Indian and Chinese emission regions have seldom been compared.

All these deserts and sandy lands are active dust sources today, with the potential to transport large quantities of mineral dust aerosols over the Asian continent and beyond. A further comparative study of their geochemical features is therefore necessary to assess past contributions to the eastern Qinghai–Tibetan Plateau or other regions. Five surface mud crusts were collected from the upper 30 cm of sandy lands in the northern Qaidam basin and Tengger, Badain Juran and North and South Taklamakan deserts (samples QD-009, TG-018, BJ-024, TK-074 and TK-103 respectively, Fig. 1) as part of a large sampling campaign of sandy deposits throughout northern China (Sun et al., 2007). Loess (samples CLS-25 and CLS-27), paleosol (CLS-29) and red clay samples (CLS-20 and CLS-90) were collected in the central loess plateau in the vicinity of the Xifeng and Bajiazui sections, which have been studied in several publications (e.g. Ding et al., 2001; Jahn et al., 2001; Xiong et al., 2010). Dune sands were collected from the surface of the Thar desert (samples TDSD-1, TDSD-2 and TDSD-3). Ten surface soils from the eastern Tibetan Plateau were also collected (samples R-1 to R-18-4) to serve as a benchmark for locally derived dust on the plateau.

The Chinese deserts were separated into five size fractions (<4, 4–16, 16–32, 32–63 and >63 μm). The coarser >32 μm fractions were separated by wet sieving and the 16–32 μm (medium silt), 4–16 μm (fine silt) and <4 μm (clay) fractions were separated using a settling method based on Stoke's Law.

2.2. Analytical methods and analysis

2.2.1. Mineralogy

Mineral proportions were measured in selected samples by X-ray diffraction at the Natural History Museum, London. The dust samples were ground in an agate mortar and loaded into a circular well mount (5 or 15 mm diameter, 1 mm depth). X-ray powder diffraction data were collected using an Enraf-Nonius PDS120 diffractometer equipped with a primary Germanium (1 1 1) monochromator and an INEL 120° curved position sensitive detector (PSD). Operating conditions for the Cu source were 40 kV and 35 mA. The horizontal slit after the monochromator was set to 0.24 mm to confine the incident beam to pure Cu Kα1 radiation. Depending on the size of the sample holder, the vertical slit was set to 1.5 (for the 5 mm well mount) or 4 mm (for the 15 mm well mount). The samples were measured in flat-plate asymmetric reflection geometry with a constant tilting angle between incident beam and sample surface of 3.5°. The sample was rotated during the measurements to improve particle counting statistics. The angular linearity of the PSD was calibrated using the external standards silver behenate and silicon (NIST SRM 640).

The whole-pattern stripping method described in Cressey and Schofield (1996) was used to derive the phase proportions. This quantification method has been successfully applied for various geological materials including dusts (LeBlond and Cressey, 2009), clay-bearing samples (Batchelder and Cressey, 1998), strongly deformed rocks (Schofield et al., 2002) and meteorites (Howard et al., 2009). The quantification of the mineral phases required external mineral standards of all identified minerals in the dust samples and appropriate standards were selected from reference materials of the mineral collection at the Natural History Museum, London and analyzed under identical run conditions as the samples. The proportion of each mineral was derived from fitting the scaling factor of the standard patterns to match corresponding peak intensities in the sample pattern. The fitted pattern of each identified standard was sequentially subtracted from that of the sample. Residual sample background levels close to zero indicated that all phases were correctly matched and stripped out. Finally, a mineral dependent absorption correction of the scaling factor yielded the weight percentages of each mineral in the samples. In some cases, the sum of the identified phases did not reach 100% (w/w) and no unassigned peaks were observed in the residual sample pattern. This likely indicates the presence of an amorphous component which proportion could be derived by difference. To assess quantification errors, best-fit scale factors were varied to some extent while inspecting the influence on the residual background. The derived estimated relative error for the mineral assemblages was 5% (w/w) for phase proportions >10% (w/w) and 10% (w/w) for phase proportions <10% (w/w).

2.2.2. Sample digestion

All work was undertaken under clean laboratory conditions (class 1000 laboratory, class 10 laminar hoods) with protective clothing and footwear. Acids used were of grade

supra-pure or purified by sub-boiling distillation. Before use, all labware was cleaned in turn with 10% v/v 8 M HCl, 10% v/v 15.6 M HNO_3 and ultrapure (Milli-Q) H_2O on a hot plate at 120 °C for 24 h each. Soil samples and dune sands from the Thar desert were first dried at 105 °C and ashed at 450 °C for 12 h each to remove any organic matter. One hundred milligrams aliquots of all desert sand and soil surface samples were then weighed into 14.7 ml screw top Savillex PTFE vessels and digested on a hot plate for 48 h in a mixture of 2 ml HF and 0.5 ml HNO_3 at 150 °C according to the digestion method described by Yu et al. (2001). All solutions were placed in an ultrasonic bath for at least 30 min at the beginning of the digestion and after 24 and 48 h. Samples were then evaporated to dryness and re-fluxed twice in 1 ml 15.6 M HNO_3 to dissolve any solid residues and fluorides that may form due to excess HF. This is important as the REE can co-precipitate with CaF_2 formed as a result of the reaction with F^- in solution and form insoluble fluorides which can affect correct REE recovery.

Four certified reference materials were used to quantify precision and accuracy of the dissolution method and test its applicability to different sample matrices. USGS BCR-1 Basalt and USGS G-2 Granite represent geological extremes of potential source mineralogy, from silica-poor (basalt) to silica-rich (granite). NIST 1515 Apple leaves and NIST 2711 Montana soil represent potential terrestrial dust archives (peat, soil profiles). In the absence of a certified peat reference material, the plant reference material NIST 1515 is often used for quality control (e.g. Weiss et al., 1999; Chen et al., 2005). NIST 1515 and NIST 2711 samples were dried and ashed following the same procedure as the dust source samples and all reference materials were then digested according to the same dissolution method. After digestion, all samples were diluted to 10 ml in 10% v/v 15.6 M HNO_3 and stored for analysis.

2.2.3. Elemental analysis

Major element concentrations were measured by ICP-AES (Varian Vista-Pro Axial) and trace element concentrations (including the REE) by quadrupole inductively coupled plasma mass spectrometry (Q-ICP-MS) using Varian ICP-MS at the Natural History Museum, London. Detection limits for all elements were calculated after each run based on the signal intensity and standard deviation measurements of the calibration blank relative to a calibration standard and were at or below the ng ml^{-1} level for all trace elements studied. Procedural blank solutions were prepared with similar acid mixtures and under identical experimental conditions as the dust source samples. Analyte concentrations in the blank solutions never exceeded the level of the detection limits.

2.2.4. Applicability of the digestion method to different sample matrices

Precision and accuracy of the digestion method were determined for each reference material. The elements of interest to us are not certified for the soil and plant reference materials used so the efficiency of digestion was tested on those elements that are presented in the certificate: Al, Cu, Fe, Pb, Rb, Ti and Zn. For USGS BCR-1 basalt and USGS G-2 granite, recoveries were compared for Al, Fe, Ti, Sc, Y, Th and the REE.

For USGS BCR-1, all elements but Ti, Gd and Tm are within 9% of the values presented in the certificate, with most within 5%. Precision errors at the 2σ level (calculated as the relative standard deviation, RSD) are less than 5% for all elements. For USGS G-2, all values but Gd, Tb and Lu are within 10% of the values presented in the certificate or in published high-precision measurements (Dulski, 2001), with most within 3%. Relative standard deviation is 8% or less for most elements, 10% for heavy REE Tm–Yb and 11% for Lu. For the soil reference material NIST 2711, all certified elements are within 9% of the certified values with RSD values below 0.3% for the major elements, 1% for Pb and 3% for Zn. The plant reference material NIST 1515 shows recoveries within 14% of the certified values for all elements but Rb. Relative standard deviations for this reference material are below 7% except for Zn (20%). However, Zn is not an element widely used in dust studies due to its potential to suffer post-depositional mobility in certain archive matrices, so this result does not affect the strength of the hot plate digestion for our purposes. The good agreement between measured and certified or published values in all reference materials shows that the dissolution method used in this study is appropriate for the digestion of mineral dust samples from a wide range of origins, including both dust sources (sand, soil) and terrestrial dust archives (peat, soil). In using a single method for the dissolution of all samples, we ensure the accurate comparison between dust source and dust receptor for the reconstruction of past atmospheric circulation patterns and palaeomonsoon dynamics on the eastern Tibetan Plateau.

3. RESULTS AND DISCUSSION

3.1. Geochemical and mineralogical characteristics of the Asian dust sources

3.1.1. Mineralogy

The mineral compositions of the <4 μm fraction of selected Chinese desert sands, loess samples from the loess plateau, dune sands from the Thar desert and Tibetan soils are given in Table 1. The fine fraction of the Chinese sands displays very high percentages of micas and clay minerals, with on average >50% illite/smectite and 10–20% muscovite (samples TG-018, BJ-024, TK-074 and TK-103). Chlorite and calcite contents are variable (1–14% and 9–22%, respectively) and quartz and feldspars are present in very low amounts (<10%). The mineralogy is likely a reflection of the grain size of the samples as weathering resistant quartz and feldspars tend to be concentrated in the coarse fractions in dust deposits while the fine fractions are enriched in micas and clays through the effect of mineral sorting during transport (Pye, 1987). Our results are in agreement with previous studies of Asian dust, which suggest that clay minerals such as illite, smectite and chlorite are enriched and quartz and feldspars depleted in the <5 μm fraction of aerosols collected above the Asian source regions (Kanayama et al., 2005) or in the <2 μm fraction of Asian

Table 1
Mineral composition (% w/w) of the Asian dust sources studied here: the Taklamakan desert of northwestern China (TK-074 and TK-103), the Tengger (TG-018) and Badain Juran deserts (BJ-024) and loess from the Chinese loess plateau (CLS-25 and CLS-27) of northern China, the Thar desert of India (TDSD-2 and TDSD-3) and soils from the eastern Qinghai–Tibetan Plateau (R1 and R15-2).

Region	Sample	Size (μm)	Qu.	Ill/Smec.	Alb.	Musc.	Chlor.	Calc.	Dolo.	Actin.
Northwestern	TK-074	<4	3	54	1	11	2	22	–	–
China	TK-103	<4	4	48	1	19	14	13	–	–
Northern	TG-018	<4	3	55	1	22	10	9	–	–
China	BJ-024	<4	6	51	1	12	1	20	–	–
	CLS-25	Bulk	20	33	5	13	5	14	–	3
	CLS-27	Bulk	19	34	8	11	5	14	–	3
India	TDSD-2	Bulk	30	20	9	8	3	10	8	10
	TDSD-3	Bulk	33	20	10	8	5	6	<1	8
Tibetan	R-1	Bulk	23	45	7	10	5	–	–	–
Plateau	R-15-2	Bulk	19	55	10	9	7	–	–	–

Qu., quartz; Ill/Smec., illite/smectite; Alb., albite; Musc., muscovite; Calc., calcite; Dolo., dolomite; Actin., actinolite.

dust deposited in Greenland (Svensson et al., 2000). Comparing the deserts to one another, the Tengger desert (TG-018) is enriched in clay minerals, muscovite and chlorite relative to the neighbouring Badain Juran desert (BJ-024). The two samples from the North and South Taklamakan desert (TK-074 and TK-103, respectively) display small variations in clay minerals (48–54%), muscovite (11–19%), chlorite (2–14%) and calcite (13–22%) contents. This desert also includes the highest observed calcite concentrations, in agreement with previous studies (Zhang et al., 2003b; Honda et al., 2004).

The loess samples (CLS-25 and CLS-27) are typically dominated by micas and clays (45–46%), followed by quartz (20%), calcite (14%) and feldspars (5–8%) and minor amounts of chlorite and mafic minerals (<5%). Quartz and feldspar concentrations are lower than typical loess, which commonly displays 50–70% quartz and 15–30% feldspar with variable quantities of micas (Xiao et al., 1995; Gallet et al., 1996; Honda et al., 2004). However, quartz and feldspar concentrations are known to decrease and micas/clays increase with decreasing size fraction in loess deposits (Eden et al., 1994; Gallet et al., 1996; Yang et al., 2006), suggesting that the loess samples may have undergone further chemical weathering and/or mineral sorting after deposition. The clay mineralogy reported in the nearby Xifeng section shows similar mineral assemblages, with illite as the most abundant clay mineral followed by lower proportions of chlorite (Jahn et al., 2001).

The soils from the Tibetan Plateau (samples R1 and R15-2) are dominated by illite/smectite (approximately 50%), and quartz (19–23%). Muscovite, chlorite and feldspars are also present in roughly equal but lower proportions. Two Tibetan soil samples from the central and northern plateau analyzed by Chang et al. (2000) display large variations in quartz (26% and 53%, respectively), feldspar (9% and 19%) and calcite (43% and 0%) contents. According to our results, calcite is not present in soils from the eastern plateau, in agreement with the northern sample, while quartz and feldspar proportions agree with those from the central soils (Chang et al., 2000). This suggests that Tibetan dust may display variable mineral assemblages and that careful sampling of the regions of interest for source tracing may be necessary for provenance studies of dust of Tibetan origin.

The two dune sands from the Thar desert (samples TDSD-2 and TDSD-3) show consistent mineral proportions, dominated by quartz (30%) and illite/smectite (20%), with lower amounts of feldspar (10%), actinolite (8–10%) and chlorite (<5%). Calcite and dolomite proportions are variable (6–10% and <1–8%, respectively). The presence of actinolite suggests that the Indian desert may be characterized by different heavy mineral assemblages to the Chinese and Tibetan sources. Amphiboles such as actinolite and other heavy minerals can be important REE hosts and such mineralogical differences may be reflected in the geochemistry. Clay minerals also have the potential to be major REE carriers (Condie, 1991) and their varying proportions in all source deposits described here may similarly lead to distinctive REE concentrations.

3.1.2. Major elements

Major element abundances of all bulk and size-separated samples are given in Table 2. Upper continental crust (UCC: Taylor and McLennan, 1985)-normalized plots are shown in Fig. 2, along with published bulk and size separated data when available for comparison. The >63 μm fraction of the Chinese deserts (this study) and corresponding published bulk samples from the Taklamakan and Tengger deserts (Honda et al., 2004) and coarse sands (>250 μm) from different locations in the northern and southern Taklamakan desert (Yang et al., 2007b) (Fig. 2A and C) are nearly identical with respect to major element characteristics. This suggests that the >63 μm fraction of the samples analyzed in this study can be directly compared to bulk samples from other deserts to assess geographical differences in major element composition.

The most notable feature of the bulk and >63 μm fraction of the Asian dust sources presented here is the large variation in CaO content. CaO is enriched relative to UCC in the Taklamakan desert and Qaidam basin sands, depleted in the Tengger and Badain Juran deserts as well as the Tibetan soils and is similar to UCC in the Thar desert (Fig. 2). The Taklamakan desert displays on average higher CaO than the Qaidam basin and Badain Juran, Tengger

Table 2
Major element composition of the Asian dust sources. Concentrations of major oxides are given in % (w/w).

Region	Sample	Size (μm)	Al_2O_3	CaO	Fe_2O_3	K_2O	MgO	MnO	Na_2O	P_2O_5	TiO_2
Northwestern China	TK-074	<4	17.33	11.44	7.69	3.53	5.02	0.111	0.720	0.096	0.574
		16–32	10.24	18.81	3.36	2.04	2.69	0.083	1.52	0.107	0.554
		>63	5.87	28.21	1.39	1.49	1.45	0.056	1.17	0.059	0.250
	TK-103	<4	15.77	8.71	7.61	2.70	4.80	0.108	0.710	0.107	0.580
		16–32	10.88	13.99	3.34	1.91	2.89	0.079	1.89	0.148	0.638
		>63	11.14	7.26	2.98	2.42	2.09	0.056	1.91	0.047	0.374
	QD-009	<4	17.51	13.28	7.46	3.52	5.10	0.139	0.714	0.141	0.626
		16–32	10.98	12.52	3.74	1.97	3.26	0.081	1.78	0.138	0.728
		>63	8.04	14.64	3.04	1.87	4.08	0.068	1.57	0.059	0.608
Northern China	TG-018	<4	17.28	9.17	7.29	3.28	6.80	0.143	0.514	0.164	0.491
		16–32	12.23	8.76	3.86	2.16	3.14	0.073	1.67	0.118	0.646
		>63	9.88	3.30	2.06	2.06	1.45	0.038	1.82	0.041	0.344
	BJ-024	<4	17.42	11.34	7.18	3.19	5.00	0.176	0.589	0.144	0.555
		16–32	11.92	11.64	4.07	1.99	3.41	0.078	1.58	0.118	0.699
		>63	10.16	2.72	2.32	2.10	1.61	0.043	1.95	0.037	0.693
India	TDSD-1	Bulk	10.34	3.13	2.82	1.64	1.03	0.061	1.80	0.061	0.537
	TDSD-2	Bulk	10.14	5.84	3.28	1.88	1.27	0.060	1.90	0.083	0.581
	TDSD-3	Bulk	10.03	4.33	2.98	1.81	1.17	0.056	2.03	0.072	0.546
Tibetan Plateau	R-1	Bulk	13.99	1.13	4.99	2.40	1.40	0.104	1.49	0.182	0.683
	R-3	Bulk	15.35	1.08	5.14	2.56	1.48	0.079	1.79	0.114	0.725
	R4-1	Bulk	14.63	0.966	4.83	2.36	1.45	0.088	1.34	0.104	0.624
	R-9-2	Bulk	15.38	1.08	5.14	2.86	1.77	0.102	1.50	0.110	0.695
	R-10	Bulk	13.98	1.11	4.74	2.47	1.43	0.104	1.28	0.210	0.662
	R-15-1	Bulk	15.02	1.18	5.29	2.38	1.54	0.110	1.47	0.145	0.724
	R-15-2	Bulk	14.77	1.23	5.23	2.40	1.53	0.111	1.36	0.181	0.703
	R-15-3	Bulk	13.67	1.10	4.89	2.16	1.34	0.098	1.40	0.224	0.673
	R-18-1	Bulk	14.56	1.08	5.08	2.42	1.49	0.094	1.38	0.209	0.694
	R-18-4	Bulk	14.95	0.928	2.72	2.38	1.31	0.028	1.73	0.069	0.723

and Thar deserts (this study; Honda et al., 2004) as well as other deserts in northern China (Honda et al., 2004). Amongst the samples for which mineralogical data was obtained (Table 1), the highest calcite content (sample TK-074) matches the highest CaO concentration (Table 2), suggesting that the CaO concentrations may be primarily a result of variations in carbonate content, at least in the <4 μm fraction.

Al_2O_3, Fe_2O_3, MnO, Na_2O, K_2O and P_2O_5 are depleted relative to UCC in the >63 μm fraction of all the Asian deserts (Fig. 2), in agreement with the results of surface sands (Honda et al., 2004; Yang et al., 2007b) and bulk suspended aerosols collected above and downwind from the dust sources (Kanayama et al., 2005). In this fraction, the northern Taklamakan desert displays the lowest Al_2O_3, Fe_2O_3, K_2O, MgO and Na_2O concentrations (Table 2, sample TK-074) and the southern Taklamakan sample the highest Al_2O_3 and K_2O (TK-103), possibly reflecting regional variations in quartz and/or phyllosilicate (chlorite, muscovite and clay minerals). On average, the >63 μm fraction of the Taklamakan desert displays similar characteristics for these elements to the other deserts and to published values of bulk and coarse sands (Fig. 2).

Still focusing on the coarse fraction and bulk samples of the desert sands, the northern Qaidam basin presents higher MgO contents than the other Asian deserts and Tibetan soils (Table 2 and Fig. 2), suggesting the presence of higher Mg-bearing mineral phases in this desert. The Qaidam basin and Badain Juran desert are also enriched in TiO_2 relative to UCC, whereas the Taklamakan and Tengger deserts are depleted in Ti (Fig. 2). This suggests that these two deposits may contain lower amounts of Ti-bearing mineral phases such as rutile. The Tibetan soils are characterized by enrichment factors (EF) ~1 for Al_2O_3, Fe_2O_3 and MnO (Fig. 2), higher than the Chinese and Indian deserts, and depleted relative to UCC but generally higher contents of K_2O than these deposits as well (Table 2 and Fig. 2). This difference between the soils and desert samples seems directly related to the mineralogical composition of the samples, as the soils contain higher amounts of clays and micas (illite, smectite, muscovite), enriched in Al_2O_3, Fe_2O_3 and K_2O (~55–64% versus 28%), and lower amounts of quartz (~19–23% versus ~30–33%) than the Thar desert (this study; Table 1) and bulk samples from the Taklamakan and Tengger deserts (Honda et al., 2004).

The effect of particle size on the major element composition can be studied in the three size fractions of the chinese desert samples (Fig. 2A–D). While the coarse fraction (>63 μm) is depleted in most elements relative to UCC, the fine fraction (<4 μm) is enriched in Al_2O_3,

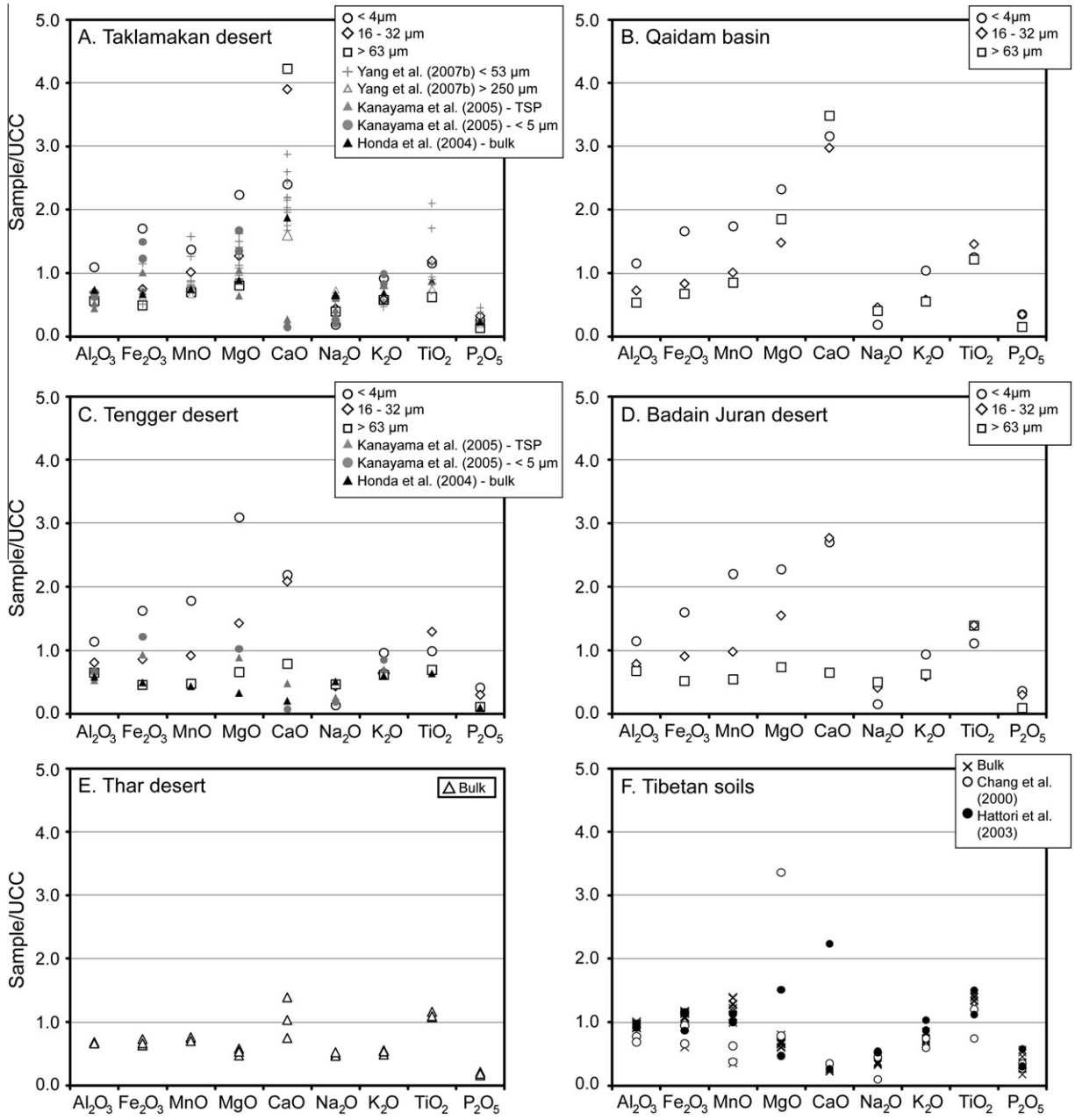

Fig. 2. UCC-normalized major element composition of three size fractions of the Asian dust sources considered (UCC: Taylor and McLennan, 1985): (A) Taklamakan desert; (B) Qaidam basin; (C) Tengger desert; (D) Badain Juran desert; (E) Thar desert and (F) soils from the eastern Tibetan Plateau. Published data of bulk and size-separated samples from the Taklamakan desert surface sands (Honda et al., 2004; Yang et al., 2007b), Tengger desert surface sands (Honda et al., 2004) and suspended aerosols downwind from the Taklamakan and Tengger deserts (Kanayama et al., 2005) are shown for comparison.

Fe_2O_3, MnO, MgO and CaO in all deserts. Similar enrichment in the finer fraction was observed in loess–paleosol and loess–red clay sequences from the Chinese loess plateau (Yang et al., 2006; Xiong et al., 2010), in the Taklamakan desert itself (Yang et al., 2007b) as well as in suspended Asian aerosols at stations downwind from the Taklamakan and Tengger deserts (Fig. 2A and C; Kanayama et al., 2005) and recovered from an ice core in Canada (Zdanowicz et al., 2006). This enrichment likely results from particle size/sorting control on mineralogy, as the fine fraction of our desert samples displayed large proportions of clay minerals, enriched in major elements such as Al_2O_3 and K_2O (illite) and Al_2O_3, MgO and Fe_2O_3 (chlorite), and very low proportions of quartz, which has a diluting effect on these elements when present in large quantities. On a plot of MgO versus Fe_2O_3 (Fig. 3), all size fractions of the Chinese deserts display a strong linear relationship ($r^2 = 0.96$, $n = 13$), suggesting that both oxides are hosted

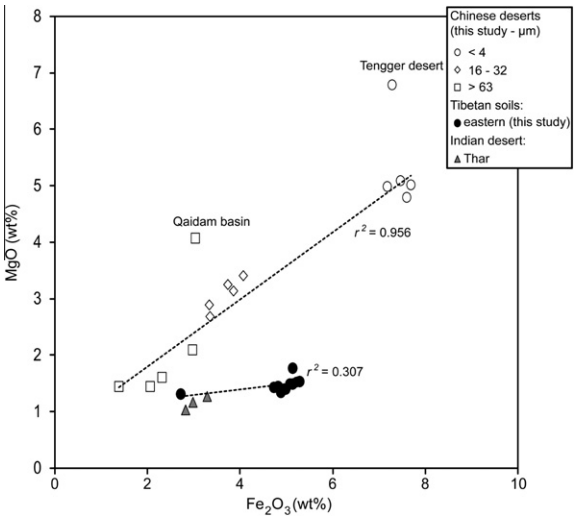

Fig. 3. Plot of MgO concentration versus Fe_2O_3 concentration in the <4 μm (open circle), 16–32 μm (open diamond) and >63 μm (open square) size fractions of the Chinese deserts, in the eastern Tibetan soils (full circles) and in the surface sands from the Thar desert (grey triangles). Oxide concentrations are given in wt.%. The r^2 values of the relationships are given.

in similar mineral assemblages in all deserts and size fractions. The higher proportion of both elements in the fine fraction likely reflects the enrichment of these mineral assemblages. Only the coarse fraction of the Qaidam basin and the fine fraction of the Tengger desert do not plot on this trend, displaying higher MgO contents relative to Fe_2O_3 and suggesting slightly different mineral controls on these two elements in those samples. The Tibetan soils plot along a different trend line and display a lower correlation ($r^2 = 0.31$, $n = 10$), suggesting that the mineral controls on both elements are different to those in the Chinese deserts.

Na_2O is higher in the coarse fraction than in the fine fraction of the desert sands (Table 2 and Fig. 2) (this study; Yang et al., 2007b), loess sequences (Yang et al., 2006; Xiong et al., 2010) and suspended aerosols (Kanayama et al., 2005). This difference may once more be linked primarily to the effect of particle size sorting during weathering, as weathering-resistant feldspars such as albite are enriched in Na_2O and concentrations of this mineral decrease with decreasing particle size. Albite contents were indeed extremely low (~1%) in the <4 μm fraction of Chinese deserts (Table 1).

P_2O_5 displays relatively little variation in the <4 μm and 16–32 μm samples as well as in the <53 μm fraction reported by Yang et al. (2007b). P_2O_5 concentrations in the >63 μm fraction of the samples analyzed in this work and the >250 μm fraction measured by Yang et al. (2007b) are lower. This suggests that the mineral assemblages controlling the presence of P_2O_5 in the smaller size fractions (possibly apatite) may be relatively independent of mineral sorting during transport. As apatite is a potential carrier of REE in Chinese loess (Gallet et al., 1996) and has been observed in minor amounts in the Taklamakan desert (Honda et al., 2004), this feature may have implications for REE provenance tracing in Asian dust.

It is worth noting that whereas the Taklamakan desert sands display large compositional variations in the coarse fraction (Table 2), the major elements are very similar in the fine <4 μm fraction of the two samples. This suggests a relative homogeneity and good mixing of the surface sands in this fine fraction, a conclusion also reached by Yang et al. (2007b). Furthermore, the similarity between the <5 μm fraction of the suspended aerosols and the corresponding <4 μm size fraction at the desert surface for the major oxides Fe_2O_3, Na_2O and K_2O (Fig. 2A and C) suggests that the fine fraction can be used as a proxy for emitted dust.

In order to compare the major element composition and weathering patterns in the silicate fraction, CaO^* is calculated on a carbonate-free basis and samples are plotted as molar proportions in a ternary Al_2O_3, $CaO^* + Na_2O$, K_2O (A–CN–K) diagram in Fig. 4 (Nesbitt and Young, 1996; Nesbitt et al., 1996). CaO^* is calculated by estimating the Ca:Na ratios of the different samples based on that of the upper continental crust (Taylor and McLennan, 1985), where $CaO^* = 0.35 \times 2 \times (\text{wt\% } Na_2O)/62$ (Nesbitt and Young, 1982; Honda and Shimizu, 1998; Honda et al., 2004). The Asian desert samples measured in this study as well as published data plot on a line parallel to Nesbitt's chemical weathering trend (Nesbitt et al., 1996). As expected, the fine (<4 μm) fraction of the Chinese desert sands plots on the high Al_2O_3 end of the trend, indicating a higher clay mineral content. Bulk samples from the Thar desert (this study) and bulk and coarse samples from the Taklamakan desert (Liu et al., 1993; Chang et al., 2000; Honda et al., 2004; Yang et al., 2007b) plot on the other end of the weathering trend. The increasing Al_2O_3 component with decreasing grain size is likely to be linked to sediment sorting during size fractionation, with quartz dilution effects in the bulk fractions and clay minerals dominating the fine weathering residues. Similar features were observed between coarser loess–paleosol and finer red clay samples of the Bajiazui sequence by Xiong et al. (2010). Fine long-range transported Asian dust aerosols are expected to plot towards the high Al_2O_3 end of the trend, along with the <4 μm samples. Indeed, Asian aerosols with a modal grain size of 4 μm and some particles >10 μm measured in a core in Canada (Zdanowicz et al., 2006) plot between the <4 and 16–32 μm fractions of our desert sands. Despite the large CaO variability observed in Table 2, it is noted that the different size classes of the Chinese desert samples all plot in narrow ranges in the A–CN–K diagram, in agreement with the idea that the CaO variability results mainly from a variation in carbonate content.

3.1.3. REE characteristics of the Asian dust sources

The REE, Sc, Y and Th concentrations of bulk samples from the different Asian dust sources are presented in Table 3. Total REE abundances vary between 126 and 130 μg g^{-1} in the Taklamakan desert and are contained within the range of published data (55−284 μg g^{-1}, Chang et al., 2000; Honda et al., 2004; Yang et al., 2007b). Abundances are slightly higher in the Qaidam basin and Badain

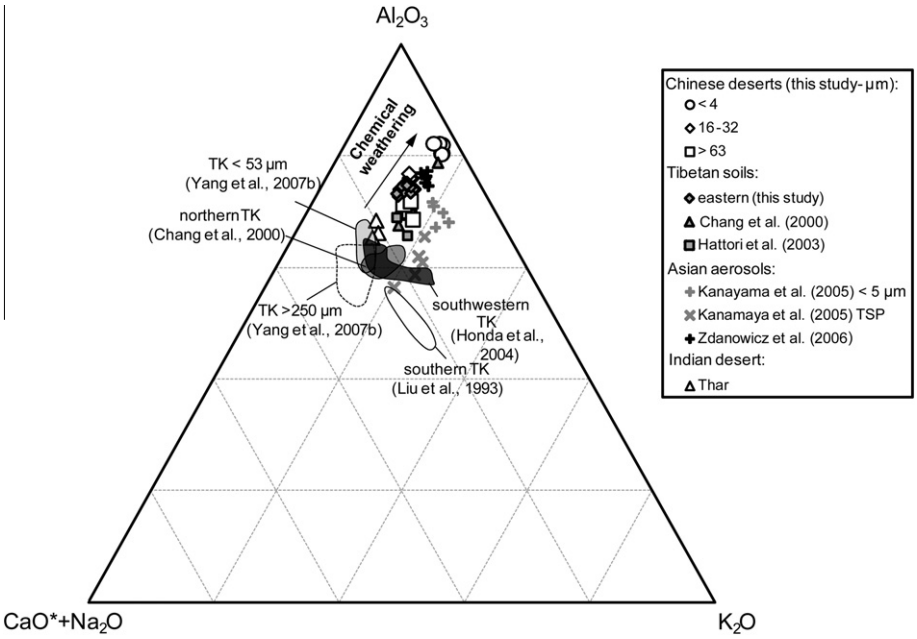

Fig. 4. A–CN–K diagram showing the relative molar proportions of Al_2O_3, $CaO^* + Na_2O$ and K_2O in the silicate fraction of the Asian dust sources considered. Published data from Tibetan soils (Chang et al., 2000; Hattori et al., 2003), Asian aerosols (Kanayama et al., 2005; Zdanowicz et al., 2006) and surface sands from the Taklamakan desert (TK, Liu et al., 1993; Chang et al., 2000; Honda et al., 2004; Yang et al., 2007b) are shown for comparison.

Juran and Tengger deserts, with total concentrations of 136–149 μg g^{-1}. Budgets are also high in the Thar desert sands (160–208 μg g^{-1}) and eastern Tibetan Plateau soils (145–188 μg g^{-1}) and variable in the Chinese loess plateau (88–161 μg g^{-1}). The latter values agree remarkably well with published results on loess–paleosol samples collected along an East–West transect across the plateau (99–170 μg g^{-1}, Jahn et al., 2001), while published compositions of soils from the northern and central Tibetan Plateau display slightly lower abundances than our data further East (91–131 μg g^{-1}, Chang et al., 2000). Yttrium abundances vary between 22 and 25 μg g^{-1} in the Chinese deserts, 16–25 μg g^{-1} in the loess section, 17–21 μg g^{-1} in the Thar desert and 20–34 μg g^{-1} in the Tibetan soils.

In order to compare the REE patterns of all Asian dust sources and discuss features which may allow the distinction between particular deposits, REE concentrations normalized to post Archean Australian shale (PAAS: Taylor and McLennan, 1985) are shown in Fig. 5. Chondrite values are frequently used as normalizing values in REE-based provenance tracing studies (e.g. Gallet et al., 1996; Pease and Tchakerian, 2002; Yang et al., 2007a,b; Wu et al., 2009a) but the resulting patterns of Asian sources are often found to present identical characteristics, with $(La/Yb)_{CH} \sim 10$ and notably $(Eu/Eu^*)_{CH} \sim 0.65$ (Ding et al., 2001; Jahn et al., 2001; Zdanowicz et al., 2006; Wu et al., 2009b). Shale-normalized patterns have been used in several dust provenance studies (Kylander et al., 2007; Zhang et al., 2009) and they were chosen over chondritic normalizations to investigate subtle differences in these crustal sources.

Most dust source samples display a slight enrichment in middle REE relative to PAAS, with varying degrees of depletion in light and heavy REE (Fig. 5). The Chinese deserts all display consistent patterns, with a positive light REE (LREE)/middle REE (MREE) slope ($[La/Gd]_{PAAS} = 0.66–0.72$), a negative MREE/heavy REE (HREE) slope ($[Gd/Yb]_{PAAS} = 1.26–1.35$) and a very slightly negative europium anomaly ($[Eu/Eu^*]_{PAAS} = Eu_{PAAS}/\sqrt{Sm_{PAAS} * Gd_{PAAS}} = 0.95–1.00$). These features are also very similar to those of the Tibetan soils ($[La/Gd]_{PAAS} = 0.60–0.80$, $[Gd/Yb]_{PAAS} = 1.28–1.57$ and $[Eu/Eu^*]_{PAAS} = 0.94–0.99$) although they present more variability in total REE budgets. These observations suggest that REE systematics alone may not be sufficient to distinguish between the Chinese deserts and Tibetan soils presented here. A combination of REE and Y, however, allows the distinction between these sources, with $[Y/La]_{PAAS} = 30.7–35.6$ and 25.2–29.2 in the Chinese deserts and Tibetan soils, respectively, excluding one soil sample displaying $[Y/La]_{PAAS} = 34.0$. Loess, paleosol and red clay samples are characterized by similar patterns to the Chinese deserts, with a positive LREE/MREE slope ($[La/Gd]_{PAAS} = 0.76–0.79$) and slightly negative MREE/HREE slope ($[Gd/Yb]_{PAAS} = 1.18–1.39$), but they are distinguished by slightly more negative europium anomalies ($[Eu/Eu^*]_{PAAS} = 0.91–0.95$). The Thar desert samples display the most distinctive REE patterns, with flatter LREE/MREE slopes ($[La/Gd]_{PAAS} = 0.77–0.91$), steeply negative MREE/HREE slope ($[Gd/Yb]_{PAAS} = 1.52–1.91$) and the most distinctive negative europium anomaly ($[Eu/Eu^*]_{PAAS} = 0.84–0.87$).

Table 3
Rare earth element, Sc, Y and Th composition of bulk samples from the different Asian dust sources (μg g^{-1}). Results for the certified reference material USGS G-2 Granite are also shown. Precision is given as the relative standard deviation (RSD) at the 2σ level ($n = 12$). Certified values from Govindaraju (1984) and results from high-precision measurements by Dulski (2001) are given for comparison. Recommended values are presented in italics.

Source area	Sample	La	Ce	Pr	Nd	Sm	Eu	Gd	Tb	Dy	Ho	Er	Tm	Yb	Lu	∑REE	Sc	Y	Th
Northwestern China																			
Taklamakan desert	TK-074	26.0	54.0	6.26	23.5	4.69	0.935	4.38	0.664	3.73	0.755	2.21	0.320	2.11	0.324	130	–	21.7	–
	TK-103	24.7	50.5	6.16	23.4	4.85	0.979	4.60	0.709	4.00	0.807	2.32	0.334	2.18	0.330	126	–	23.1	–
Qaidam basin	QD-009	29.3	59.4	7.21	27.2	5.46	1.07	5.11	0.780	4.38	0.879	2.53	0.362	2.35	0.358	146	–	25.0	–
Northern China																			
Tengger desert	TG-018	27.0	55.5	6.69	25.2	5.07	1.02	4.72	0.720	4.05	0.820	2.39	0.343	2.25	0.343	136	–	22.9	–
Badain Juran desert	BJ-024	30.0	60.3	7.32	27.9	5.52	1.13	5.14	0.772	4.26	0.852	2.46	0.352	2.30	0.350	149	–	24.0	–
Loess	CLS-25	21.2	49.8	5.05	18.9	3.70	0.678	3.33	0.496	2.96	0.592	1.67	0.247	1.61	0.240	111	7.74	16.9	7.99
	CLS-27	30.3	60.7	7.23	26.8	5.27	0.971	4.72	0.681	3.98	0.794	2.23	0.328	2.14	0.326	146	13.1	23.6	11.0
Paleosol	CLS-29	33.0	67.0	7.98	30.1	5.79	1.05	5.12	0.733	4.24	0.820	2.36	0.340	2.23	0.342	161	13.6	24.6	12.2
Red clay	CLS-20	18.4	35.7	4.30	16.0	3.19	0.620	2.96	0.447	2.68	0.543	1.58	0.232	1.51	0.227	88	9.08	16.1	5.83
	CLS-90	30.4	62.0	7.40	27.5	5.34	0.990	4.77	0.685	4.04	0.807	2.28	0.342	2.21	0.334	149	14.1	23.6	11.9
Tibetan Plateau	R-1	34.0	69.3	8.26	31.0	6.12	1.17	5.47	0.800	4.29	0.840	2.41	0.343	2.26	0.341	167	12.1	22.9	13.0
	R-3	36.6	74.7	9.10	34.6	6.99	1.37	6.38	0.953	5.20	1.03	2.92	0.429	2.74	0.419	183	13.1	27.4	14.0
	R4-1	37.7	67.5	9.44	37.4	7.93	1.63	7.71	1.13	6.05	1.18	3.31	0.458	2.97	0.452	185	13.7	33.6	13.0
	R-9-2	34.7	70.6	8.50	32.4	6.42	1.29	5.94	0.893	4.88	0.968	2.80	0.402	2.61	0.398	173	13.6	26.2	13.3
	R-10	29.5	62.6	7.22	26.8	5.25	1.03	4.69	0.706	3.90	0.781	2.25	0.326	2.13	0.324	148	12.4	20.6	12.5
	R-15-1	33.0	69.0	8.01	29.7	5.80	1.11	5.13	0.769	4.18	0.820	2.38	0.342	2.26	0.339	163	13.2	21.8	13.8
	R-15-2	31.6	66.0	7.63	28.4	5.49	1.06	4.90	0.745	4.10	0.819	2.38	0.345	2.23	0.339	156	12.7	21.3	13.7
	R-15-3	31.5	63.6	7.72	29.1	5.75	1.10	5.25	0.784	4.33	0.855	2.48	0.354	2.30	0.350	155	11.7	22.4	12.8
	R-18-1	29.6	60.7	7.16	26.5	5.05	0.967	4.51	0.685	3.80	0.765	2.23	0.328	2.14	0.327	145	12.5	20.1	12.9
	R-18-4	37.8	73.5	9.48	37.1	7.56	1.53	7.05	1.02	5.49	1.08	3.03	0.426	2.72	0.415	188	13.2	28.9	14.8
Indian Thar desert	TDSD-1	45.2	89.4	10.3	38.4	7.13	1.22	6.05	0.835	4.22	0.797	2.16	0.306	1.92	0.279	208	8.84	20.7	18.5
	TDSD-2	37.7	76.7	9.20	34.2	6.96	1.15	5.97	0.849	4.66	0.875	2.34	0.331	2.07	0.308	183	7.92	19.0	17.2
	TDSD-3	34.0	64.1	8.49	31.1	6.17	1.02	5.00	0.723	4.13	0.798	2.18	0.316	1.99	0.291	160	7.78	17.0	13.0
Reference material																			
This study ($n = 12$)	USGS G-2	84.2	154	15.8	53.3	7.41	1.4	5.54	0.582	2.19	0.359	0.879	0.111	0.679	0.09	–	4.13	9.50	25.7
RSD (2σ, %)		7.9	6.22	8.08	5.56	6.74	5.85	4	6.09	6.45	7.2	8.13	9.22	9.71	10.87	–	7.99	6.00	4.22
Govindaraju (1984)	USGS G-2	89	160	*18*	55	7.2	1.4	*4.3*	*0.48*	2.4	*0.4*	*0.92*	*0.18*	0.8	*0.11*	–	3.5	11	24.7
RSD (2σ, %)		18	13		22	19	17			25				50			0.4	2	
Dulski (2001)	USGS G-2	87	158	16.3	51.5	6.8	1.41	4.1	0.49	2.08	0.35	0.88	0.117	0.72	0.12	–		9.4	–

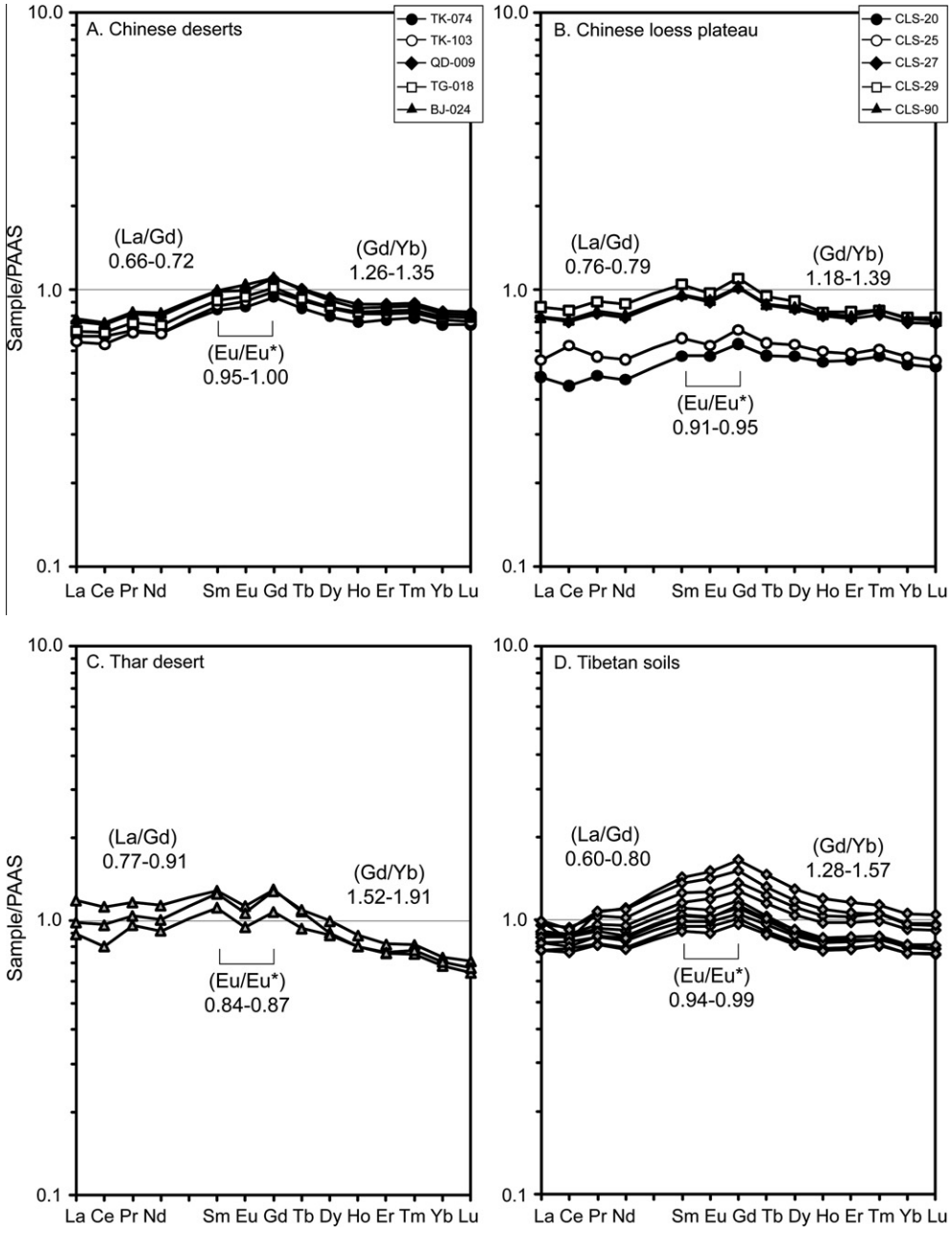

Fig. 5. Post Archean Australian shale-normalized REE patterns for bulk samples of the Asian dust sources considered: (A) the Chinese deserts; (B) the Chinese loess plateau; (C) the Thar desert and (D) the Tibetan soils (PAAS: Taylor and McLennan, 1985).

3.2. Particle size considerations for REE-based provenance tracing

Particle size can have an important effect on the REE budget of crustal rocks (McLennan, 1989). Studies of Asian surface sands have shown that REE concentrations vary greatly with size fraction (Chang et al., 2000; Honda et al., 2004; Yang et al., 2007a,b) but suspended aerosols collected at stations around the Chinese deserts and loess–paleosol samples in the Chinese loess plateau have shown similar REE concentrations irrespective of size fraction (Ding et al., 2001; Kanayama et al., 2005). REE patterns themselves are often found to be independent of particle diameter (Yang et al., 2007a,b). These differences have important implications for REE-based provenance tracing as only certain particle sizes can be transported regionally and globally and the correct size fraction in the source region must be analyzed for accurate comparisons with dust archives to be made. Here, we study the changes in trace and REE budgets and patterns as well as REE-based provenance tracers in five size classes of the different Chinese deserts, and investigate which size fraction in the sources will best represent the geochemistry of aerosols transported to the eastern Tibetan Plateau.

3.2.1. Particle size effects and controls on trace and REE concentrations

Rare earth element, Sc, Y and Th concentrations in all size fractions of the Chinese deserts samples are presented in Table 4 and UCC-normalized values for all grain sizes are shown in Fig. 6. The most striking effect of grain size on the REE composition of the Chinese desert samples is the difference between the <32 and the >32 μm fractions (Fig. 6). While the two coarse fractions (32–63 and >63 μm) are generally depleted relative to UCC, the <32 μm fractions all display enrichment relative to crustal values, notably of the MREE (Eu–Dy). Rare earth element concentrations are generally slightly lower in the clay fraction (<4 μm) than in the medium and fine silt fractions (4–32 μm) except for the Tengger desert. Despite having different REE budgets, all size fractions, and notably the <4 μm and 4–16 μm classes, have similar patterns, in agreement with published studies (Yang et al., 2007a,b). The disparity between the <32 and >32 μm fractions is also characterized by different Y budgets (Fig. 6), which are generally enriched relative to UCC in the <32 μm size class but depleted in the >32 μm fraction. Given these observations, it seems that the mineral hosts of Y and the REE are depleted in the coarser grains. In Fig. 7, all samples irrespective of size display a linear relationship ($r^2 = 0.947$, $n = 15$) on a plot of $\sum$REE versus Y (Fig. 7A), suggesting similar mineralogical controls on their concentration in all size classes despite different abundances.

Scandium and Th however show more variation, with a strong enrichment in the <4 μm fraction, near crustal values in the 16–32 μm fraction and a depletion in the >63 μm samples (Fig. 6A–D). The mineral hosts of these two elements seem to be predominantly concentrated in the clay fraction. Indeed, a plot of $\sum$REE versus Th and Sc (Fig. 7B) shows that the 4 μm fractions plots off the linear array formed by the 16–32 and >63 μm fractions ($r^2 = 0.814$ and 0.949 for Sc and Th, respectively, $n = 10$). This suggests that the controls on Sc and Th contents are different in the fine fraction to those of the medium and coarse fractions. Figs. 7C and D show the correlation between total REE budgets and concentrations of P_2O_5 and TiO_2, respectively. While the REE show a strong correlation with P_2O_5 in all fractions ($r^2 = 0.866$, $n = 15$), correlation with TiO_2 is only observed in the 16–32 μm fraction, where it is remarkably high ($r^2 = 0.984$, $n = 5$). This suggests that Ti-bearing phases such as rutile may concentrate REE only in the medium silt fraction, while minerals such as apatite are potential important hosts of REE in these Chinese deserts, irrespective of size fraction.

The decrease in REE abundance with increasing grain size has been observed in several studies of REE in Asian deserts (Honda et al., 2004; Yang et al., 2007a,b) and loess deposits worldwide (Gallet et al., 1998). As proposed previously on the basis of mineralogy and major element composition, this difference seems linked to mineral proportions. The fine fractions contain little quartz and feldspars, which are depleted in REE (Taylor and McLennan, 1985), and abundant clay minerals, which have the potential to be major carriers of REE in certain sedimentary rocks (Condie, 1991). Despite their low trivalent REE content, feldspars can be important hosts of Eu (Taylor and McLennan, 1985) and tend to concentrate this element in the coarser fraction. Indeed, the coarse and fine particles are characterized by different Eu anomalies, negative in the finer <32 μm fractions and positive in the >63 μm fraction (Fig. 6).

Bulk samples are generally enriched relative to UCC (Fig. 6A–D), with REE budgets plotting closest and displaying similar patterns to the <4 μm size class. Whereas the major elements in the >63 μm size class gave a good representation of the bulk geochemistry of the desert sands, it seems that the <4 μm fraction is the best representative of the REE composition of bulk samples and that REE budgets are controlled by more complex mineral phases which do not show a linear response to grain size. Published bulk values collected in the Taklamakan desert by Honda et al. (2004) also plot within the finer fractions (Fig. 6A). Their relatively wide spread of values encompasses all the samples with a size range of <32 μm. Both total suspended particulates and <5 μm aerosols collected downwind from the Taklamakan and Tengger deserts (Kanayama et al., 2005) also plot amidst the <32 μm samples (Fig. 6A and C).

3.2.2. Which particle size for the provenance tracing of Asian dust over the eastern Tibetan Plateau?

During strong dust storms such as those affecting the deserts of northern and northwestern China in spring and the Thar desert in summer, the entire range of particle sizes is emitted from the source regions (Marticorena et al., 1997). While the larger particles are quickly re-deposited through the effect of gravitational settling (Marticorena et al., 1997; Zhang et al., 1997), the finer particles are lifted into the lower and upper troposphere and transported regionally and globally (Zhang et al., 1997; Sun et al., 2001; Wu et al., 2009a). Before choosing a particular size fraction at the surface of the dust sources to be compared with the dust recovered from a climate archive in the region of interest, the size of the dust effectively reaching the archive must be measured or estimated.

When meteorological stations exist in the vicinity of the study area and dust aerosols are directly collected, this question can be easily addressed. Unfortunately, such stations are not in place in all regions, notably in remote areas such as the eastern Tibetan Plateau, where direct measurements of suspended aerosols are not available. The dust particle size reaching such regions must thus be estimated. Measuring this directly in the archive is not always straightforward as local or proximal dust sources may also be active which will deposit both coarse and fine dust and interfere with the long-range signal. Therefore, the likely size of the deposited aerosols must be assessed based on studies of regionally and long-range transported aerosols.

Asian dust particles transported to Greenland have diameters between 0.1 and 5 μm (Biscaye et al., 1997; Svensson et al., 2000) and those recovered from an ice core in Canada have also been shown to exhibit modal diameters of 4 μm (Zdanowicz et al., 2006), suggesting that the <4 μm fraction is characteristic of long-range transported dust. Even in regions closer to the source areas, such as the study of a snow field in Japan, it was found that particles <4 μm best represented the deposited Asian dust (Osada et al.,

Table 4
Rare earth element, Sc, Y and Th concentrations in the <4, 4–16, 16–32, 32–63 and >63 μm size fractions of the Chinese dust sources. Concentrations are given in μg g^{-1}.

Source area	Sample	Size (μm)	La	Ce	Pr	Nd	Sm	Eu	Gd	Tb	Dy	Ho	Er	Tm	Yb	Lu	Sc	Y	Th
Northwestern China																			
Taklamakan desert	TK-074	<4	26.8	59.0	6.52	24.4	4.80	0.947	4.42	0.661	3.70	0.748	2.23	0.324	2.17	0.335	17.3	21.8	15.6
		4–16	27.6	55.6	6.56	24.5	4.93	0.975	4.59	0.698	3.94	0.796	2.31	0.333	2.18	0.336	–	23.0	–
		16–32	25.5	50.8	6.31	24.0	4.93	0.986	4.79	0.740	4.16	0.838	2.43	0.349	2.26	0.342	10.0	22.7	9.14
		32–63	16.7	31.7	3.99	15.2	3.07	0.677	2.94	0.445	2.52	0.507	1.45	0.207	1.34	0.201	–	14.9	–
		>63	13.6	24.8	3.21	12.1	2.47	0.578	2.46	0.389	2.26	0.461	1.32	0.187	1.19	0.178	4.54	12.9	3.52
	TK-103	<4	21.3	47.6	5.64	21.5	4.43	0.864	4.14	0.652	3.73	0.773	2.32	0.341	2.29	0.351	16.5	21.6	14.4
		4–16	30.2	60.4	7.35	27.8	5.67	1.11	5.29	0.790	4.40	0.872	2.47	0.352	2.29	0.342	–	25.2	–
		16–32	28.3	57.1	7.10	27.2	5.75	1.14	5.61	0.890	5.03	1.02	2.93	0.421	2.72	0.411	10.5	29.1	11.2
		32–63	18.8	37.1	4.59	17.5	3.59	0.785	3.43	0.529	2.99	0.607	1.74	0.247	1.62	0.246	–	17.6	–
		>63	12.8	25.5	3.11	11.8	2.41	0.623	2.29	0.352	1.99	0.399	1.17	0.169	1.12	0.168	8.32	11.5	4.99
Qaidam basin	QD-009	<4	32.4	66.6	7.80	29.2	5.72	1.08	5.35	0.807	4.52	0.913	2.64	0.383	2.50	0.383	17.7	26.1	18.5
		4–16	35.2	70.9	8.55	31.9	6.38	1.20	5.89	0.895	4.99	0.995	2.87	0.406	2.64	0.399	–	28.4	–
		16–32	34.2	70.0	8.61	32.9	6.68	1.28	6.26	0.961	5.37	1.08	3.09	0.442	2.88	0.441	11.3	30.3	12.1
		32–63	24.8	49.7	6.18	23.4	4.76	0.953	4.48	0.696	3.99	0.794	2.32	0.337	2.18	0.327	–	22.9	–
		>63	19.9	39.8	4.97	19.0	3.85	0.845	3.68	0.559	3.17	0.640	1.82	0.258	1.66	0.254	7.61	17.8	5.78
Northern China																			
Tengger desert	TG-018	<4	32.3	70.4	7.97	30.2	6.07	1.17	5.56	0.845	4.67	0.944	2.75	0.393	2.61	0.398	17.6	27.6	18.9
		4–16	32.2	65.4	7.94	29.7	5.99	1.16	5.56	0.840	4.71	0.947	2.75	0.391	2.54	0.387	–	27.2	–
		16–32	29.5	59.6	7.41	28.2	5.71	1.13	5.52	0.858	4.91	0.996	2.90	0.420	2.73	0.418	11.9	26.1	11.0
		32–63	22.4	44.5	5.52	21.0	4.32	0.917	4.05	0.627	3.67	0.748	2.16	0.316	2.08	0.320	–	20.6	–
		>63	16.9	33.6	4.19	15.7	3.06	0.684	2.79	0.422	2.35	0.478	1.41	0.203	1.34	0.203	6.96	12.6	6.02
Badain Juran desert	BJ-024	<4	33.7	69.4	8.21	31.1	6.06	1.20	5.55	0.832	4.50	0.905	2.60	0.374	2.45	0.377	18.8	26.2	15.3
		4–16	36.9	73.2	8.92	34.3	6.79	1.34	6.32	0.931	5.12	1.01	2.90	0.408	2.65	0.399	–	28.9	–
		16–32	31.6	64.3	8.06	30.8	6.30	1.28	6.07	0.936	5.28	1.06	3.07	0.440	2.88	0.439	12.4	28.4	10.9
		32–63	19.6	38.8	4.79	18.0	3.66	0.821	3.41	0.521	2.98	0.607	1.73	0.252	1.65	0.251	–	16.7	–
		>63	14.2	27.8	3.43	13.0	2.52	0.643	2.38	0.366	2.10	0.428	1.27	0.190	1.25	0.192	7.14	11.5	5.35

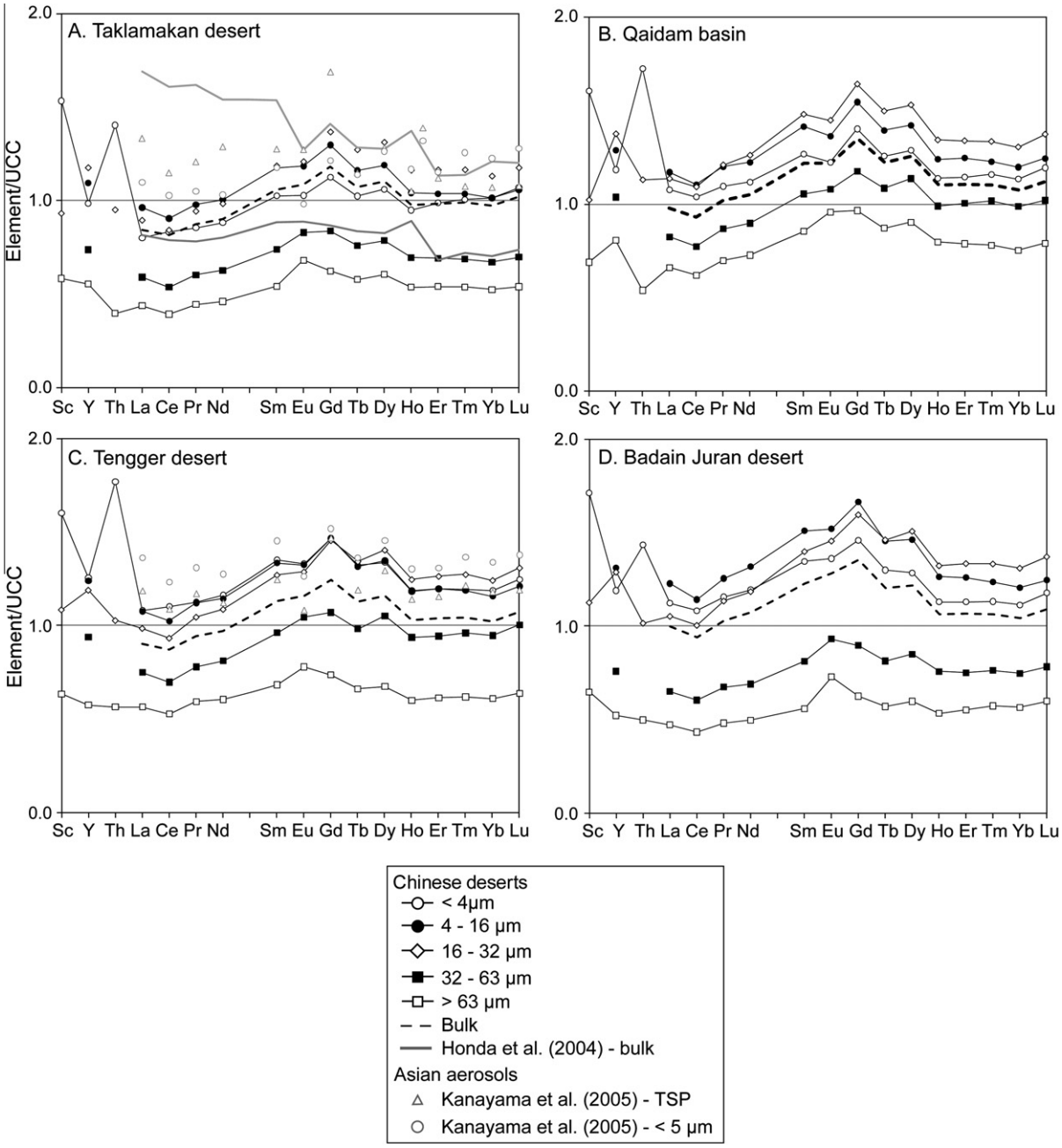

Fig. 6. UCC-normalized REE, Sc, Y and Th composition in five size fractions and bulk samples of the Chinese deserts (UCC: Taylor and McLennan, 1985): (A) the Taklamakan desert; (B) the Qaidam basin; (C) the Tengger desert and (D) Badain Juran desert. Published data for Taklamakan desert surface sands (upper and lower limit of the range of published values given by a grey line, Honda et al., 2004), and suspended aerosols downwind from the Taklamakan and Tengger deserts (Kanayama et al., 2005) are shown for comparison.

2004). Particles transported regionally may also include larger diameters and Zhang et al. (2003b) found that particles <16 μm made up 70% of the total atmospheric dust loading in Asia. A mixture of dust with median grain sizes of 3 and 15 μm was also found in Korean aerosols (Lee et al., 2010) and particles with mean diameters of 12–13 μm were recovered in Beijing after a particularly strong dust storm (Yang et al., 2007a). In this view, particle sizes with diameters <16 μm are likely to best represent dust transported regionally over Asia and to the eastern Tibetan Plateau, and the <4–5 μm (Zdanowicz et al., 2006; Chen et al., 2007) or <16 μm fractions (Sun et al., 2007) are commonly used in provenance tracing studies over Asia and the Pacific ocean. We choose to use the <4 μm fraction of the Chinese deserts to represent long-range transported dust from these sources as data from the 4–16 μm fraction is not available for all elements. Based on Fig. 6, REE patterns for the <4 and 4–16 μm fractions were nearly identical, suggesting that REE-based provenance tracers will be similar in both classes. Indeed, $[La/Gd]_{PAAS} = 0.63–0.74$ and 0.70–0.73,

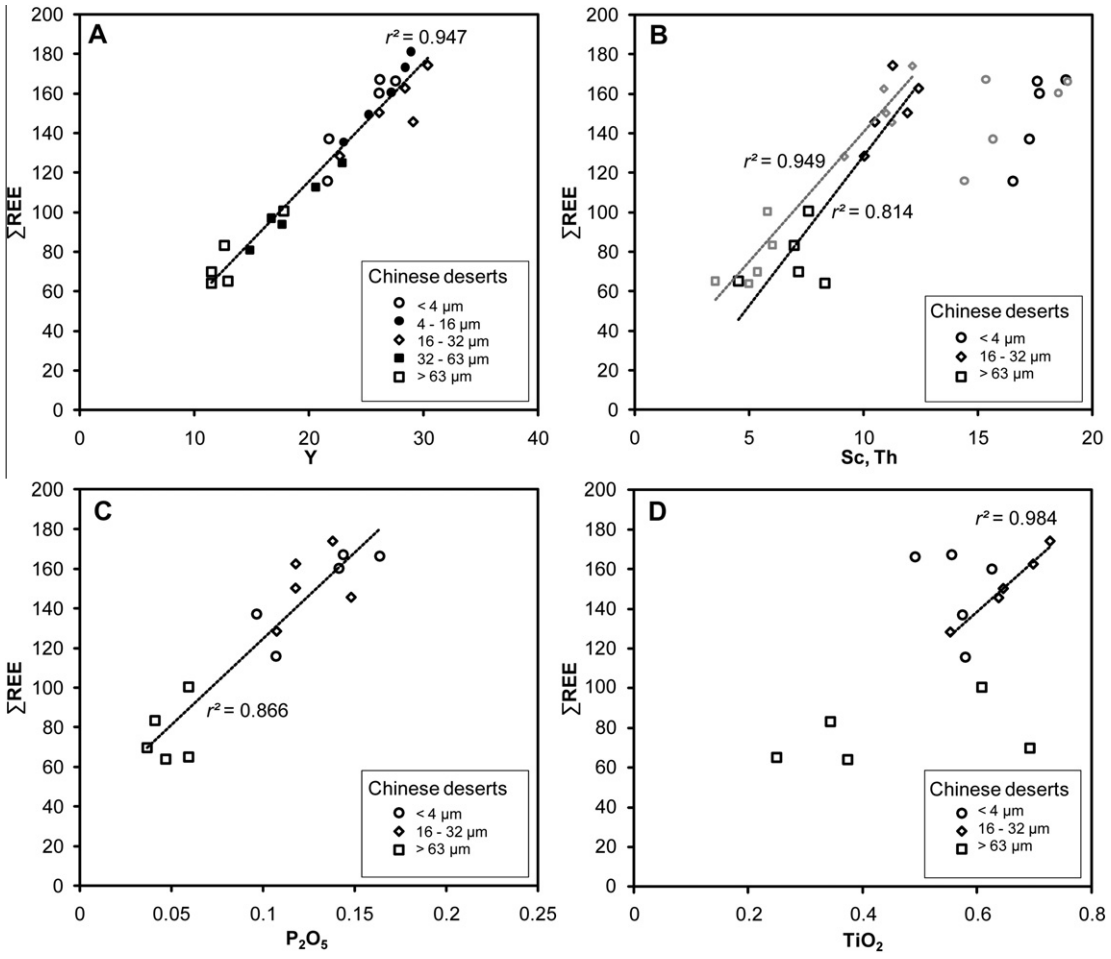

Fig. 7. Relationships between the concentrations of: (A) ∑REE versus Y; (B) ∑REE versus Sc (black open shapes) and versus Th (grey open shapes); (C) ∑REE versus P_2O_5; and (D) ∑REE versus TiO_2 for different size fractions of the Chinese desert surface samples. The r^2 values of the relationships are given on each plot. REE, Y, Sc and Th values are given in μg g^{-1}, P_2O_5 and TiO_2 values are given in wt.%.

$[Gd/Yb]_{PAAS} = 1.09–1.37$ and 1.27–1.44 and the europium anomaly $[Eu/Eu^*]_{PAAS} = 0.92–0.97$ and 0.92–0.97, respectively, for the <4 and 4–16 μm classes of the Chinese deserts measured.

3.2.3. Particle size effects on dust provenance tracers

For provenance tracing of dust, elemental ratios are useful and more representative than individual concentrations in the distinction between aeolian dust sources. They omit dilution effects of certain minerals and allow the combination of different trends in rare earth element and trace element patterns. Fig. 8 examines the effect of particle size on various provenance tracing ratios in all size fractions of the Chinese desert sands. Proxies involving Th or Sc are shown in the >63, 16–32 and <4 μm fractions only as data for these elements is not available in the other classes. Published data from suspended aerosols is also included when available. We notably seek to answer two questions. First, are any provenance tracers independent of grain size? If so, they can be applied to dust sources and archives regardless of the size fraction of transported dust. This could be useful when size separated data is unavailable in the source regions. Second, are provenance tracers measured in the surface sands representative of those measured in suspended aerosols above the source regions? If this is the case, the assumption that surface sands can be directly compared to the dust particles analyzed in a climate archive is indeed warranted.

Size-independent proxies have been studied in previous work on Asian dust but are so far limited to the major element-based proxy $[CaO + Na_2O + MgO]/TiO_2$ (Yang et al., 2006) and Nd isotopes (e.g. Kanayama et al., 2005). Ratios such as La/Th, Th/∑REE, Y/Yb, Sc/La and Th/Tb are clearly dependent on particle size (Fig. 8), while others display nearly identical values in all classes of our desert samples. Indeed, Y/∑REE, La/Er, La/Gd, Gd/Er, La/Yb, Y/Tb, Y/La and Y/Nd show little or no variation between the five size fractions presented. The europium anomaly Eu/Eu^* only displays very slight enrichments in the coarse fraction relative to the medium and fine fraction due to the higher concentration of feldspars as discussed previously. The ratios Th/Sc and Y/Yb are independent of size fraction for particle sizes <32 μm. Many of these size-independent proxies relate to the shape of the REE-patterns and show that although REE budgets may vary between different size fractions, the REE patterns do

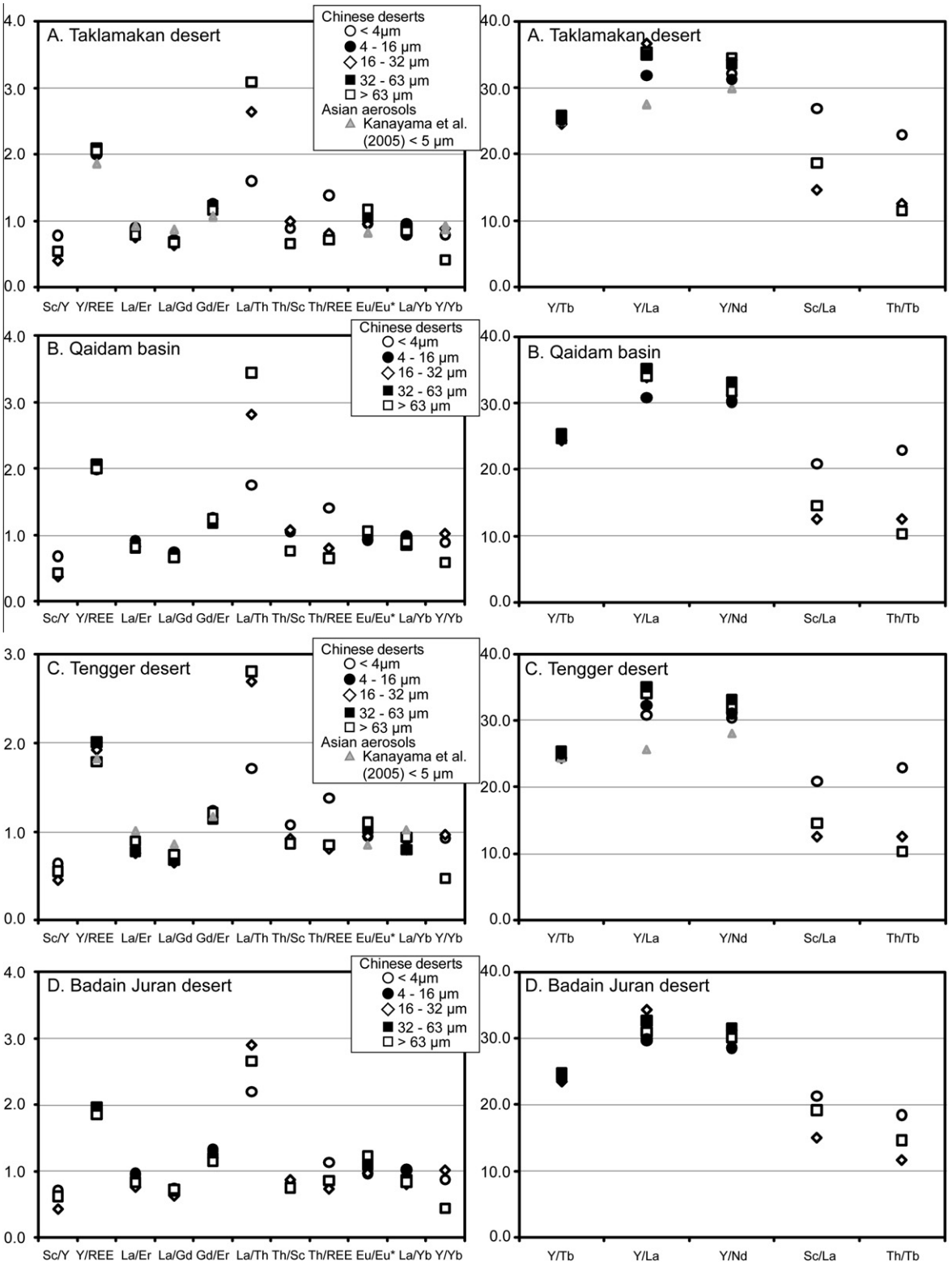

Fig. 8. Effect of particle size on various trace and REE-based provenance tracers in surface samples from: (A) the Taklamakan desert; (B) the Qaidam basin; (C) the Tengger desert and (D) the Badain Juran desert. Also shown for comparison are the <5 μm size fraction of suspended aerosols downwind from the Taklamakan and Tengger deserts (grey triangles, Kanayama et al., 2005). All REE values are normalized to PAAS (PAAS: Taylor and McLennan, 1985).

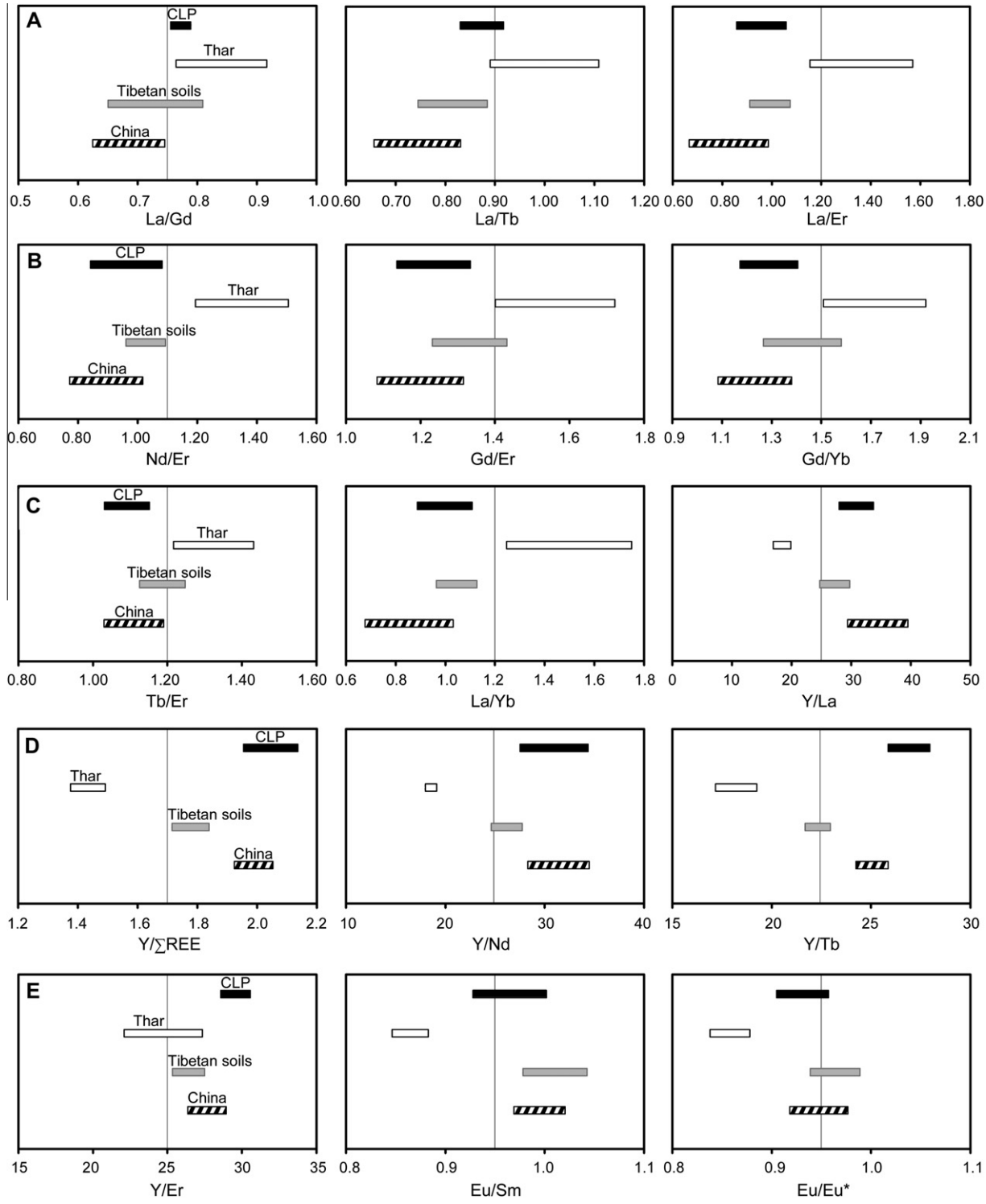

Fig. 9. Range of signatures of various trace and REE-based provenance tracers in the <4 μm of the Chinese deserts ($n = 5$); the Tibetan soils ($n = 9$); the Chinese loess plateau (CLP, $n = 5$); and the Thar desert ($n = 3$). Compositional ranges between the Thar desert and the remaining sources should only be compared using the size-independent ratios: La/Gd and La/Er (A), Gd/Er (B), La/Yb and Y/La (C), Y/∑REE, Y/Nd and Y/Tb (D), and Eu/Eu* (E). Preference is given to provenance tracers which display restricted and non-overlapping ranges within each source domain. All REE values are normalized to PAAS (PAAS: Taylor and McLennan, 1985).

not, as suggested based on the UCC-normalized patterns in Fig. 6. It can therefore be concluded that the PAAS-normalized REE-based proxy ratios Y/∑REE, La/Er, La/Gd, Gd/Er, La/Yb, Y/Tb, Y/La and Y/Nd and to a certain extent the europium anomaly Eu/Eu* are useful size independent provenance tracers which can be used to trace

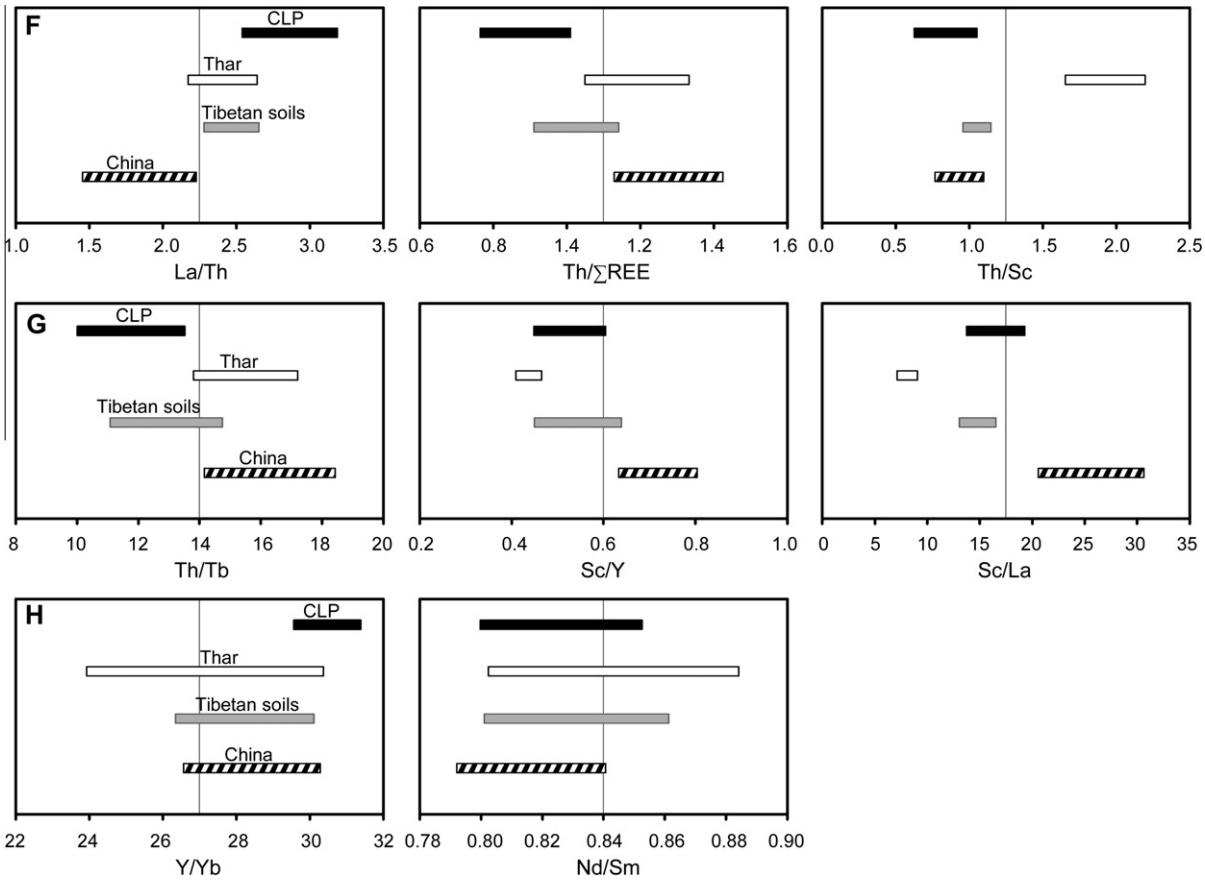

Fig 9. *(continued)*

the origin of deposited dust to various Asian source regions even when only bulk source samples are available. Given that this is the case for our surface samples from the Thar desert (Table 3), these proxies will be useful in the subsequent assessment of dust provenance to the eastern Tibetan Plateau. Furthermore, all proxies are identical in both the <4 μm and 4–16 μm fractions, comforting the idea that the <4 μm clay fraction, when available, can be taken as representative of both regionally and long-range transported dust.

Comparing the <4 μm fraction of our surface sands from the Taklamakan and Tengger deserts to available data for the <5 μm fraction of suspended aerosols collected downwind from these sources (Fig. 8A and C, Kanayama et al., 2005), it can be seen that the fine fraction of the surface sands and the suspended aerosols display nearly identical results for all available provenance ratios. Only results for Y/La and Y/Nd present small differences between surface samples and aerosols ($[Y/La]_{PAAS} = 35$ and 27, respectively, for the Taklamakan desert and $[Y/La]_{PAAS} = 33$ and 26 for the Tengger desert) but the latter still plot closest to the <4 μm fraction. It therefore seems that all trace and REE-based provenance tracers measured at the surface of the Chinese deserts are reasonable representations of the suspended aerosols available for transport to the eastern Tibetan Plateau and other regions.

3.3. Provenance tracing of Asian dust to the eastern Tibetan Plateau

The best provenance tracers for the study of Asian dust transported to the eastern Tibetan Plateau are determined here. Specifically, provenance tracers are sought, which will allow: (i) the distinction between Chinese versus Indian dust input, as this will have implications for the dominant hemispheric wind currents affecting this region and (ii) the distinction between different Chinese dust sources (e.g. northwestern versus northern deserts, Chinese loess plateau), as this will allow the study of regional wind currents such as the northerly winter monsoon or the Westerly jet. Any combination of two rare earth element and trace element-based elemental ratios has the potential to discriminate between the dust sources of interest as long as they display significant enough differences between them.

Fig. 9A–H displays the geochemical signature of different groups of potential dust sources to the eastern Tibetan Plateau for a number of trace element and REE provenance tracers. For the Chinese deserts, Chinese loess plateau and Tibetan soils, the selected samples were chosen to represent the particle sizes which would effectively be transported to and deposited on the eastern Tibetan Plateau: (a) the <4 μm fraction is chosen to represent long-range transported dust from the Chinese deserts as discussed in

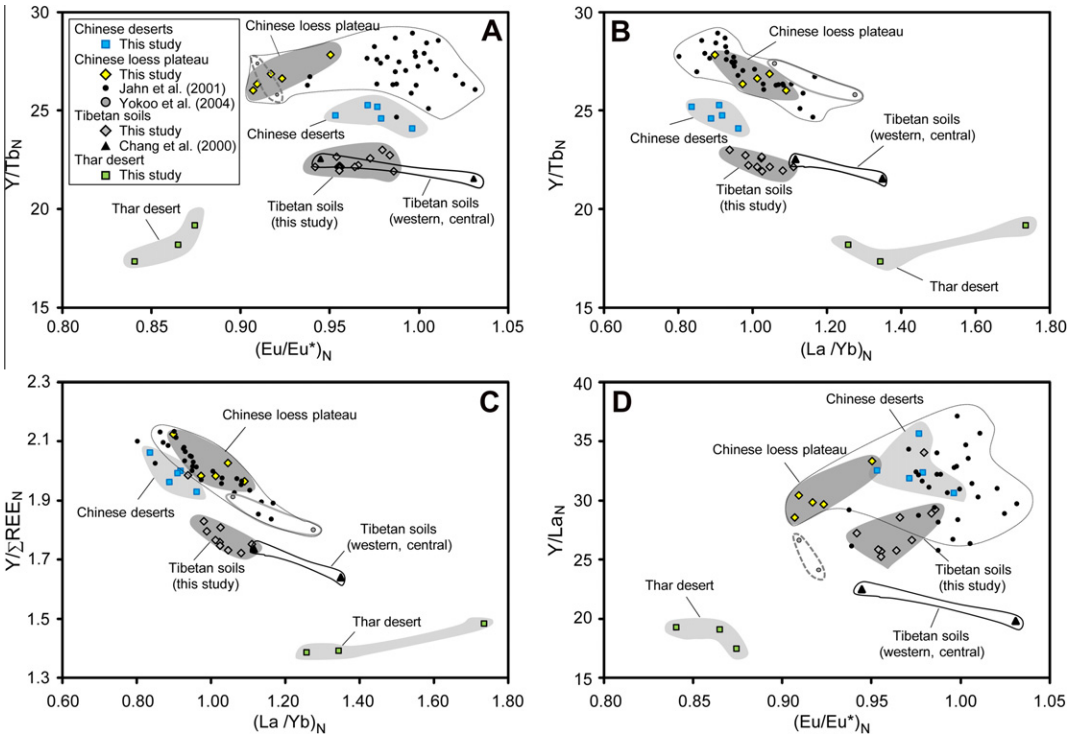

Fig. 10. Bivariate plots of: (A) Y/Tb_N versus $(Eu/Eu^*)_N$; (B) Y/Tb_N versus $(La/Yb)_N$; (C) $Y/\sum REE_N$ versus $(La/Yb)_N$ and (D) Y/La_N versus $(Eu/Eu^*)_N$ for the bulk surface samples from the Chinese sources (Qaidam basin and Taklamakan, Tengger and Badain Juran deserts), the Thar desert, eastern (this study) and western and central Tibetan soils (Chang et al., 2000) and samples from the Chinese loess plateau (this study; Jahn et al., 2001; Yokoo et al., 2004). The *N* subscript indicates that values are normalized to PAAS (PAAS: Taylor and McLennan, 1985).

Section 3.2.2; (b) as loess represents reworked aeolian material already previously emitted, transported and deposited, we propose that bulk loess samples can be used to represent deposition from this regional source; and (c) the Tibetan soils were collected and analyzed to represent local dust deposition on the eastern Tibetan Plateau. Given the proximity of these samples to the proposed region of study and absence of long-range transport, size segregation during transport is unlikely to occur and bulk samples are chosen to represent this local source. It is therefore proposed that these three sources (the Chinese deserts, Chinese loess plateau and Tibetan soil end-members) can be compared using any provenance tracers in Fig. 9 as they are comprised of sample sizes which have the potential to reach a dust archive on the eastern Tibetan Plateau. The direct comparison between the signature of these sources and the Thar desert, however, is only justifiable for the size-independent tracers and this source is plotted on all figures for information only. When choosing two ratios for the distinction of a particular source or group of sources, one must ensure that the signature of the different sources overlaps as little as possible and that their geochemical signature within each source is as confined as possible.

3.3.1. Provenance tracers for hemispheric dust transport to the Tibetan Plateau: Indian versus Chinese dust

It was shown that the proxy ratios $Y/\sum REE$, La/Er, La/Gd, Gd/Er, La/Yb, Y/Tb, Y/La, Y/Nd and to a certain extent the europium anomaly Eu/Eu^* are useful size independent provenance tracers which represent long-range transported dust even when bulk samples are used. Given that no size separated samples are available for the Thar desert, bulk compositions of all dust sources are compared using these particular ratios. Specifically, combinations of proxies are sought, which can successfully distinguish Thar desert sands from those of the Chinese sources as well as from the local signature of the Tibetan soils.

Of these proxies, all ratios but La/Gd (Fig. 9A) allow a clear definition of the Indian signature. Four bivariate plots using various combinations of the remaining size-independent proxies are shown in Fig. 10A–D. The pairs $Y/Tb–Eu/Eu^*$, Y/Tb–La/Yb, $Y/\sum REE–La/Yb$ and $Y/La–Eu/Eu^*$ are successful in distinguishing Thar desert dust, which consistently plots away from the various Chinese deposits. The eastern Tibetan soils are separated from the Chinese and Indian sources on all plots, suggesting that these geochemical proxies will also allow to distinguish local from long-range dust contributions to the eastern Tibetan Plateau. Furthermore, published values of soils from the central and northern Plateau (Chang et al., 2000) plot in the vicinity of the eastern soils analyzed in this study and away from the Chinese deserts, suggesting that these combinations of tracers could potentially be extended to the study of the entire Tibetan Plateau. The plot of Y/Tb versus Eu/Eu^* (Fig. 10A) is particularly useful for tracing dust of Tibetan origin.

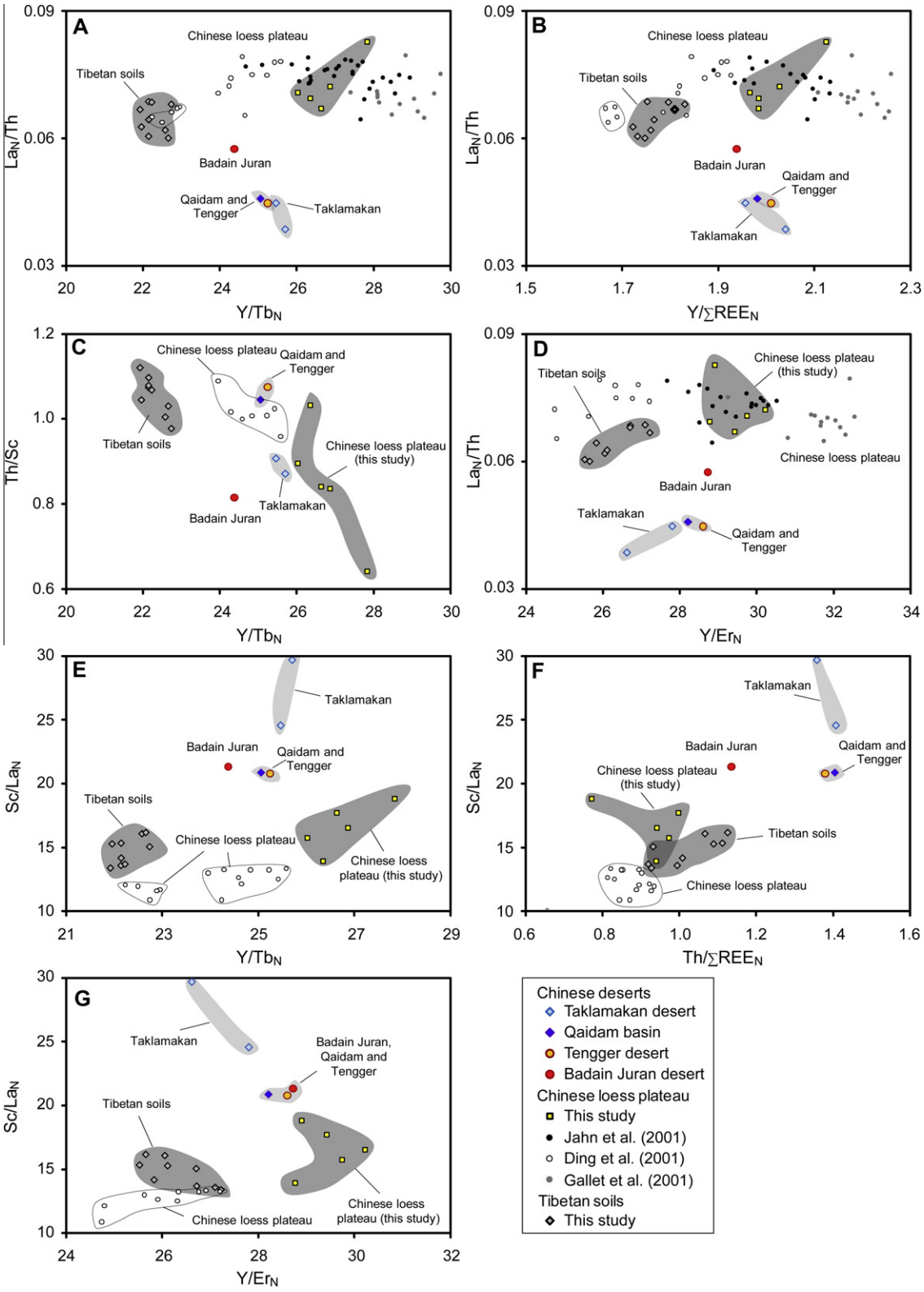

Fig. 11. Bivariate plots of: (A) La$_N$/Th versus Y/Tb$_N$; (B) La$_N$/Th versus Y/$\sum$REE$_N$; (C) Th/Sc versus Y/Tb$_N$; (D) La$_N$/Th versus Y/Er$_N$; (E) Sc/La$_N$ versus Y/Tb$_N$; (F) Sc/La$_N$ versus Th/$\sum$REE$_N$ and (G) Sc/La$_N$ versus Y/Er$_N$ showing domains for the <4 μm fraction of the Qaidam basin and Taklamakan, Tengger and Badain Juran deserts, the eastern Tibetan soils and Chinese loess plateau. Published loess data from Jahn et al. (2001), Ding et al. (2001) and Gallet et al. (1996) are shown for comparison. The *N* subscript indicates that values are normalized to PAAS (PAAS: Taylor and McLennan, 1985).

The loess samples agree well with published data (Jahn et al., 2001; Yokoo et al., 2004) and the signature of this Chinese dust source can be further separated from that of the different deserts based on combinations of Y/Tb, Eu/Eu* and La/Yb (Fig. 10A and B). Therefore, it seems that combinations of Y/Tb–Eu/Eu*, Y/Tb–La/Yb, Y/∑REE–La/Yb and Y/La–Eu/Eu* provide useful frameworks for the study of aeolian transport from the Thar desert, the Tibetan Plateau and the Chinese dust sources. The combinations of Y/Tb–Eu/Eu* and Y/Tb–La/Yb further allow the distinction of clear domains for dust originating from the Chinese loess plateau and the deserts of northern and northwestern China.

3.3.2. Provenance tracers for regional dust transport: distinguishing the Chinese dust sources

As discussed previously, all proxies can be used to compare Chinese and Tibetan dust sources as the samples were selected to best characterize those transported to the eastern Tibetan Plateau. Based on Fig. 9D, the provenance tracer Y/Tb is very well suited for the study of Asian dust as there is no or very little overlapping between the different sources and each group presents a fairly restricted compositional range. Y/∑REE and Y/Nd (Fig. 9D) are equally well suited although the individual source compositions are not as restricted. La/Th and Th/∑REE (Fig. 9F) allow a good discrimination of the Chinese loess plateau and Chinese deserts and Sc/La (Fig. 9G) of the latter alone. The Y/Er (Fig. 9E) and Th/Sc (Fig. 9F) compositions of the different sources are not as distinct but each source is relatively well confined. Different combinations of these proxies are therefore chosen to establish which combinations of provenance tracers are suited for the distinction between different Chinese deserts, the Chinese loess plateau and the local Tibetan soils.

Fig. 11A–G displays a series of seven bivariate plots based on these elemental proxies. All provenance tracer pairs and especially La/Th–Y/Tb, La/Th–Y/∑REE, La/Th–Y/Er and Sc/La–Y/Tb (Fig. 11A, B, D and E) can be used to distinguish between the Tibetan soils, the Chinese loess plateau (this study; Gallet et al., 1996; Ding et al., 2001; Jahn et al., 2001) and the combined Chinese deserts. Of these tracers, La/Th and Sc/La can be used to separate the signature of the Chinese deserts from that of the Chinese loess plateau and Y/Tb and Y/∑REE from the Tibetan soils.

Within the Chinese deserts, the Taklamakan and Tengger deserts and the Qaidam basin are indistinguishable based on La/Th, Y/Tb and Y/∑REE (Fig. 11A and B) but the proxy Y/Er presents a slight division (Fig. 11D). Despite their overlapping characteristics, the signature of these three deserts is clearly distinct from that of the other sources. In all plots but Sc/La–Y/Tb and Sc/La–Y/Er (Fig. 11E and G), the Badain Juran desert plots away from the remaining deposits and the distinction of this desert is best made using the proxies La/Th and Th/∑REE. In a plot of Th/Sc versus Y/Tb (Fig. 11C), Th/Sc allows to further separate the signatures of the Tengger desert and Qaidam basin from that of the Taklamakan desert. In this case, however, the loess deposits are not as well constrained by this tracer and plot very near the Taklamakan domain. In Fig. 11E and F, the combination of Sc/La, Y/Tb and Th/∑REE allows the clearest distinction between the Chinese deserts. In these figures, and notably Fig. 11F, the Taklamakan desert, the Badain Juran desert and the combined Tengger desert and Qaidam basin plot in separate domains, suggesting that Sc/La and Th/∑REE combined may be useful provenance tracers for the distinction between these different deserts. The Tibetan soils and loess samples, however, plot on overlapping domains in Fig. 11F. Fig. 11G shows that the combination of Sc/La and Y/Er could be useful in distinguishing dust from the Taklamakan desert, although the remaining Chinese deserts all plot in the same area.

These seven bivariate plots present clear distinctions between the Tibetan soils, Chinese loess plateau and combined Chinese deserts. Between them they further allow the refining and separation of fields from the Taklamakan and Badain Juran deserts. The provenance tracers established here will thus prove to be useful for the provenance tracing of dust deposited to the eastern Tibetan Plateau, but also to other regions where the specific source of Chinese dust is to be investigated.

3.3.3. Further implications for the source of aeolian deposits

Geochemical proxy combinations such as those obtained in Figs. 10 and 11 for the different Asian dust sources are not only useful for the tracing of atmospheric dust transported over Asia and beyond, but also for the study of the provenance and history of the aeolian deposits themselves. For instance, the thick loess–paleosol sequence of central China offers an unequalled potential to study aeolian deposition and environmental change in the past 2.6 Ma (Liu and Ding, 1998; Xiong et al., 2010), but debate concerning its origin still exists (Gallet et al., 1996; Ding et al., 1998, 2001; Jahn et al., 2001). It is generally accepted, based on similarities in the REE and Sr–Nd isotope characteristics of loess deposits within China and worldwide, that they are sourced from

Table 5
Comparison of loess compositions in different regions.

	$(La/Gd)_{PAAS}$	$(Gd/Yb)_{PAAS}$	$(La/Yb)_{PAAS}$	$(Eu/Eu^*)_{PAAS}$	La/Th
Chinese loess plateau					
This study	0.78–0.79	1.29–1.35	0.97–1.09	0.91–0.92	2.7–2.8
Published[a]	0.65–0.82	1.07–1.45	0.74–1.17	0.94–1.05	2.4–3.7
Beijing loess[b]	0.61–0.88	0.99–2.51	0.68–1.38	–	2.6–5.3
Argentinean loess[c]	0.62–0.75	1.11–1.25	0.69–0.85	0.94–1.05	2.4–3.2

[a] Ding et al. (2001) and Jahn et al. (2001).
[b] Yang et al. (2007a).
[c] Gallet et al. (1998).

aeolian material having undergone multiple phases of sedimentary recycling and mixing (Taylor et al., 1983; Gallet et al., 1998; Jahn et al., 2001; Honda et al., 2004). Results from our loess and paleosol samples agree well with previously published results in the Chinese loess plateau (Ding et al., 2001; Jahn et al., 2001), Argentina (Gallet et al., 1998) and loess deposits north of Beijing (Yang et al., 2007a) (Table 5), in agreement with the idea of a well-mixed source of loess.

It has also been suggested that a wind-blown source could have been sustained for the past ca. 7 Ma based on the observation that REE (except cerium) are consistent in loess and paleosol layers, as well as in the underlying red clay deposits (Ding et al., 2001). Our loess, paleosol and red clay samples also display consistent REE and trace element characteristics (Table 3 and Figs. 10, 11), providing a small amount of additional data to support this interpretation although more samples are needed.

The source of this aeolian material has also long been debated. While earlier work suggested that the loess deposits could be derived from material in the Tarim basin and Taklamakan desert (Liu et al., 1993), more recent studies have proposed that they may rather originate from deposits in northern China such as the Badain Juran and Tengger deserts, the Qaidam basin and the Gobi desert in southern Mongolia (Chen et al., 2007; Sun et al., 2008). It seems that the data presented here would agree with the latter hypothesis based on the location of the loess and desert domains in Fig. 11. Though this interpretation is rather speculative and more data from the northern deserts are needed to verify this on the bivariate plots, the loess samples plot closer to the Qaidam basin and Badain Juran and Tengger deserts than the Taklamakan end-member in all but Fig. 11C. In Fig. 11G notably, the proximity between the loess samples and these three desert sources is more visible.

Certain loess and paleosol samples analyzed by Ding et al. (2001) along a North–South transect of the Chinese loess plateau plot away from the remaining loess samples and amidst the domain of the Tibetan soils (Fig. 11A, B and E). These samples correspond to the loess unit L1-5 and underlying paleosol unit S1 of the neighbouring Wupu, Yanchang and Yichuan sections and could suggest that the Tibetan Plateau is a possible source of loess material to central China. In an investigation of the source of material to the Taklamakan desert, Chang et al. (2000) found that Tibetan soils were a possibility based on similarities in their REE characteristics. Though tentative, our data suggests that Tibetan soils could be a potential source for loess deposits as well.

Samples from the Qaidam basin and Tengger deserts consistently plot together in all provenance tracing plots in Fig. 11. Whereas certain elemental proxies distinguish the other Asian sources, these two deposits have remarkably similar REE and trace element characteristics, suggesting the possibility of a common source of material for these two deserts.

4. CONCLUSIONS

Surface samples from some of the major Asian dust sources in China and India were analyzed for their mineralogical and elemental composition. The goal of this study was to provide a geochemical framework of elemental characteristics and provenance indicators for the accurate provenance tracing of dust particles from these different sources, with a particular emphasis on the tracing of dust transported to the eastern Tibetan Plateau. The main conclusions are:

(1) Clay minerals, followed by quartz and feldspars, are the main constituents of samples from the Chinese loess plateau and soils from the eastern Tibetan Plateau. The fine fraction of surface samples from the Chinese deserts is dominated by clays and other sheet silicates, with very low contents of quartz and feldspars, reflecting the effect of mineral sorting during size separation. Dune sands from the Thar desert display quartz as their primary mineral phase, followed by clays and feldspars. Calcite contents are highly variable in all Asian dust sources, from below detection limit in the Tibetan soils to over 20% in the Taklamakan desert.

(2) Major element composition of coarse and bulk sands from the different deserts reflect their mineralogy: they are depleted in Al_2O_3, Fe_2O_3, MnO, Na_2O, K_2O and P_2O_5 relative to UCC and present variable CaO contents. The fine fraction of the Chinese deserts is enriched in Al_2O_3, Fe_2O_3, MnO, MgO and K_2O relative to the coarse fraction but depleted in Na_2O, likely reflecting the enrichment in clay minerals and depletion in Na-bearing feldspars in this fraction. While regional heterogeneity is found in the coarse fraction of the Taklamakan desert sands, the fine fraction is more homogeneous and suggests a good mixing of the finer particles at the surface of this desert, in agreement with previous work. Analysis of CaO in the silicate fraction shows very little variability, suggesting that most of the CaO in the dust sources can be attributed to variations in calcite content. CaO concentrations must thus be treated with care if they are to be used as provenance indicators of transported dust.

(3) Rare earth element concentrations are similar in all Asian dust sources, varying between ~90 and 210 $\mu g\ g^{-1}$. Post Archean Australian shale (PAAS)-normalized REE patterns of the Thar desert in India are different to those of the Chinese and Tibetan sources, with steeper HREE slopes ($[Gd/Yb]_{PAAS} =$ 1.52–1.91 against 1.18–1.57) and more negative europium anomalies ($[Eu/Eu^*]_{PAAS} = 0.84–0.87$ against 0.91–1.00), suggesting that the REE are useful provenance indicators for dust from the Thar desert. Rare earth element patterns alone cannot distinguish between the Chinese deserts, loess or Tibetan soils, suggesting that combinations with other trace elements are needed to find source specific provenance tracers for these sources. The ratio Y/La is for example useful in discriminating between the Chinese deserts and Tibetan soils. Analysis of REE and trace element concentrations and patterns in different size fractions of the Chinese sands shows that the

<32 μm fraction is enriched in REE and Y relative to the >32 μm fraction and generally to UCC, in agreement with previous studies. Despite different REE budgets, UCC-normalized patterns are similar in all size fractions, with en enrichment in middle-REE. This similarity is best observed between the <4 μm and 4–16 μm classes. Bulk samples have similar abundances and patterns to the <4 μm fraction.

(4) The ratios $Y/\sum REE_{PAAS}$, $(La/Er)_{PAAS}$, $(La/Gd)_{PAAS}$, $(Gd/Er)_{PAAS}$, $(La/Yb)_{PAAS}$, Y/Tb_{PAAS}, Y/La_{PAAS}, Y/Nd_{PAAS} and to a certain extent the europium anomaly $(Eu/Eu^*)_{PAAS}$ are independent of size class in the Chinese desert samples and can thus be used to study the regional or long-range transport of Asian dust even when only bulk samples are available in the source region. Th/Sc and Y/Yb_{PAAS} are independent of particle size for samples <32 μm. The <4 μm and 4–16 μm fractions are nearly identical with respect to all provenance tracers studied, suggesting that these two size fractions can be equally used to study the long-range transport of Asian dust and specifically to the eastern Tibetan Plateau. The size independent proxies $Y/\sum REE_{PAAS}$, $(Gd/Er)_{PAAS}$, $(Eu/Eu^*)_{PAAS}$, $(La/Yb)_{PAAS}$, Y/Tb_{PAAS}, Y/La_{PAAS} and Y/Nd_{PAAS} are useful provenance tracers for dust transported from the Thar desert. The proxy combinations Y/Tb_{PAAS}–$(Eu/Eu^*)_{PAAS}$, Y/Tb_{PAAS}–$(La/Yb)_{PAAS}$, $Y/\sum REE_{PAAS}$–$(La/Yb)_{PAAS}$ and Y/La_{PAAS}–$(Eu/Eu^*)_{PAAS}$ in bivariate plots not only display a clear geochemical domain for the Indian source but also separate the Tibetan soils, Chinese loess plateau and Chinese deserts. Though these proxies cannot distinguish between the individual Chinese deserts themselves, they can be applied to any study seeking to establish the regional origin of transported dust. Y/Tb_{PAAS} is the best suited tracer for the distinction between these different sources, presenting both confined signatures within each source and clear distinctions between them.

(5) Combinations of La_{PAAS}/Th, Y/Tb_{PAAS}, $Y/\sum REE_{PAAS}$, Sc/La_{PAAS} and Y/Er_{PAAS} allow to clearly distinguish dust from the Tibetan soils, the Chinese loess plateau and the Chinese deserts. For the study of individual Chinese deserts, La_{PAAS}/Th and $Th/\sum REE_{PAAS}$ allow the distinction of the Badain Juran desert, Th/Sc is useful in isolating the signature of the Qaidam and Tengger deserts from the Taklamakan and Badain Juran deserts and the combination of Sc/La_{PAAS} and Y/Er_{PAAS} separates the Taklamakan desert from the remaining dust sources. The proxy combinations Sc/La_{PAAS}–Y/Tb_{PAAS} and Sc/La_{PAAS}–$Th/\sum REE_{PAAS}$ are useful for distinguishing dust from the different Chinese deserts considered here.

(6) The agreement between the loess, paleosol and red clay data with published values is in line with previous interpretations that these deposits likely originate from a well-mixed crustal source having undergone several sedimentary cycles and that the aeolian deposition could have been sustained for the past several million years. Similarities between the eastern Tibetan soils and published data from the central loess plateau could point towards a Tibetan source for the loess deposits, although more data is required. The nearly indistinguishable signature of the samples from the northern Qaidam basin and the Tengger desert in all identified proxies suggests that the Qaidam sandy land and the neighbouring Tengger desert may share a common source of material.

ACKNOWLEDGMENTS

We express our gratitude to Catherine Unsworth for her technical aid and expertise and David Large and Baruch Spiro for their involvement. We are grateful to three anonymous reviewers for providing very constructive and helpful comments regarding our previous manuscript submission. This work was made possible by financial support from Imperial College, the Department of Earth Sciences and Engineering and the Natural History Museum, London, and the "One-hundred Talents" program of the Chinese Academy of Sciences (to Youbin Sun).

REFERENCES

An Z. S., Porter S. C., Kutzbach J. E., Wu X. H., Wang S. M., Liu X. D., Li X. Q. and Zhou W. J. (2000) Asynchronous Holocene optimum of the East Asian monsoon. *Quatern. Sci. Rev.* **19**, 743–762.

Batchelder M. and Cressey G. (1998) Rapid, accurate phase quantification of clay-bearing samples using a position-sensitive X-ray detector. *Clay Clay Mineral.* **46**, 183–194.

Biscaye P. E., Grousset F. E., Revel M., VanderGaast S., Zielinski G. A., Vaars A. and Kukla G. (1997) Asian provenance of glacial dust (stage 2) in the Greenland Ice Sheet Project 2 Ice Core, Summit, Greenland. *J. Geophys. Res.: Oceans* **102**, 26765–26781.

Bory A. J. M., Biscaye P. E. and Grousset F. E. (2003) Two distinct seasonal Asian source regions for mineral dust deposited in Greenland (NorthGRIP). *Geophys. Res. Lett.* **30**.

Carrico C. M., Bergin M. H., Shrestha A. B., Dibb J. E., Gomes L. and Harris J. M. (2003) The importance of carbon and mineral dust to seasonal aerosol properties in the Nepal Himalaya. *Atmos. Environ.* **37**, 2811–2824.

Chang Q., Mishima T., Yabuki S., Takahashi Y. and Shimizu H. (2000) Sr and Nd isotope ratios and REE abundances of moraines in the mountain areas surrounding the Taklimakan Desert, NW China. *Geochem. J.* **34**, 407–427.

Chen B., Krachler M., Gonzalez Z. I. and Shotyk W. (2005) Improved determination of arsenic in environmental and geological specimens using HG-AFS. *J. Anal. At. Spectrom.* **20**, 95–102.

Chen F. H., Yu Z. C., Yang M. L., Ito E., Wang S. M., Madsen D. B., Huang X. Z., Zhao Y., Sato T., Birks H. J. B., Boomer I., Chen J. H., An C. B. and Wunnemann B. (2008) Holocene moisture evolution in arid central Asia and its out-of-phase relationship with Asian monsoon history. *Quatern. Sci. Rev.* **27**, 351–364.

Chen J., Chen Y., Liu L. W., Ji J. F., Balsam W., Sun Y. B. and Lu H. Y. (2006) Zr/Rb ratio in the Chinese loess sequences and its implication for changes in the East Asian winter monsoon strength. *Geochim. Cosmochim. Acta* **70**, 1471–1482.

Chen J., Li G. J., Yang J. D., Rao W. B., Lu H. Y., Balsam W., Sun Y. B. and Ji J. F. (2007) Nd and Sr isotopic characteristics of Chinese deserts: implications for the provenances of Asian dust. *Geochim. Cosmochim. Acta* **71**, 3904–3914.

Condie K. C. (1991) Another look at rare-earth elements in shales. *Geochim. Cosmochim. Acta* **55**, 2527–2531.

Cressey G. and Schofield P. F. (1996) Rapid whole-pattern profile stripping method for the quantification of multiphase samples. *Powder Diffract.* **11**, 35–39.

Ding Z. L., Sun J. M., Yang S. L. and Liu T. S. (1998) Preliminary magnetostratigraphy of a thick eolian red clay-Loess sequence at Lingtai, the Chinese Loess Plateau. *Geophys. Res. Lett.* **25**, 1225–1228.

Ding Z. L., Sun J. M., Yang S. L. and Liu T. S. (2001) Geochemistry of the Pliocene red clay formation in the Chinese Loess Plateau and implications for its origin, source provenance and paleoclimate change. *Geochim. Cosmochim. Acta* **65**, 901–913.

Dulski P. (2001) Reference materials for geochemical studies: new analytical data by ICP-MS and critical discussion of reference values. *Geostand. Newsl.: J. Geostand. Geoanal.* **25**, 87–125.

Dykoski C. A., Edwards R. L., Cheng H., Yuan D. X., Cai Y. J., Zhang M. L., Lin Y. S., Qing J. M., An Z. S. and Revenaugh J. (2005) A high-resolution, absolute-dated Holocene and deglacial Asian monsoon record from Dongge Cave, China. *Earth Planet. Sci. Lett.* **233**, 71–86.

Eden D. N., Wen Q. Z., Hunt J. L. and Whitton J. S. (1994) Mineralogical and geochemical trends across the loess plateau, North China. *Catena* **21**, 73–90.

Fleitmann D., Burns S. J., Mudelsee M., Neff U., Kramers J., Mangini A. and Matter A. (2003) Holocene forcing of the Indian monsoon recorded in a stalagmite from Southern Oman. *Science* **300**, 1737–1739.

Gallet S., Jahn B. M. and Torii M. (1996) Geochemical characterization of the Luochuan loess–paleosol sequence, China, and paleoclimatic implications. *Chem. Geol.* **133**, 67–88.

Gallet S., Jahn B. M., Lanoe B. V., Dia A. and Rossello E. (1998) Loess geochemistry and its implications for particle origin and composition of the upper continental crust. *Earth Planet. Sci. Lett.* **156**, 157–172.

Govindaraju K. (1984) 1984 compilation of working values and sample description for 170 international reference samples of mainly silicate rocks and minerals. *Geostand. Newsl.* **8**, 3.

Hattori Y., Suzuki K., Honda M. and Shimizu H. (2003) Re–Os isotope systematics of the Taklimakan Desert sands, moraines and river sediments around the Taklimakan Desert, and of Tibetan soils. *Geochim. Cosmochim. Acta* **67**, 1195–1205.

Honda M. and Shimizu H. (1998) Geochemical, mineralogical and sedimentological studies on the Taklimakan Desert sands. *Sedimentology* **45**, 1125–1143.

Honda M., Yabuki S. and Shimizu H. (2004) Geochemical and isotopic studies of aeolian sediments in China. *Sedimentology* **51**, 211–230.

Howard K. T., Benedix G. K., Bland P. A. and Cressey G. (2009) Modal mineralogy of CM2 chondrites by X-ray diffraction (PSD-XRD): Part 1. Total phyllosilicate abundance and the degree of aqueous alteration. *Geochim. Cosmochim. Acta* **73**, 4576–4589.

Husar R. B., Tratt D. M., Schichtel B. A., Falke S. R., Li F., Jaffe D., Gasso S., Gill T., Laulainen N. S., Lu F., Reheis M. C., Chun Y., Westphal D., Holben B. N., Gueymard C., McKendry I., Kuring N., Feldman G. C., McClain C., Frouin R. J., Merrill J., DuBois D., Vignola F., Murayama T., Nickovic S., Wilson W. E., Sassen K., Sugimoto N. and Malm W. C. (2001) Asian dust events of April 1998. *J. Geophys. Res.: Atmos.* **106**, 18317–18330.

Jahn B. M., Gallet S. and Han J. M. (2001) Geochemistry of the Xining, Xifeng and Jixian sections, Loess Plateau of China: eolian dust provenance and paleosol evolution during the last 140 ka. *Chem. Geol.* **178**, 71–94.

Kanayama S., Yabuki S., Yanagisawa F. and Motoyama R. (2002) The chemical and strontium isotope composition of atmospheric aerosols over Japan: the contribution of long-range-transported Asian dust (Kosa). *Atmos. Environ.* **36**, 5159–5175.

Kanayama S., Yabuki S., Zeng F. J., Liu M. Z., Shen Z. B., Liu L. C., Yanagisawa F. and Abe O. (2005) Size-dependent geochemical characteristics of Asian dust – Sr and Nd isotope compositions as tracers for source identification. *J. Meteorol. Soc. Jpn.* **83A**, 107–120.

Kang S. C., Mayewski P. A., Qin D. H., Sneed S. A., Ren J. W. and Zhang D. Q. (2004) Seasonal differences in snow chemistry from the vicinity of Mt. Everest, central Himalayas. *Atmos. Environ.* **38**, 2819–2829.

Kylander M. E., Muller J., Wust R. A. J., Gallagher K., Garcia-Sanchez R., Coles B. J. and Weiss D. J. (2007) Rare earth element and Pb isotope variations in a 52 kyr peat core from Lynch's Crater (NE Queensland, Australia): proxy development and application to paleoclimate in the Southern Hemisphere. *Geochim. Cosmochim. Acta* **71**, 942–960.

LeBlond J. S. and Cressey G. (2009) A rapid method for quantifying single mineral phases in heterogeneous natural dusts using X-ray diffraction. *Powder Diffract.* **24**, 17–23.

Lee M. K., Il Lee Y. and Yi H. I. (2010) Provenances of atmospheric dust over Korea from Sr–Nd isotopes and rare earth elements in early 2006. *Atmos. Environ.* **44**, 2401–2414.

Liu T. S. and Ding Z. L. (1998) Chinese loess and the paleomonsoon. *Annu. Rev. Earth Planet. Sci.* **26**, 111–145.

Liu C. Q., Masuda A., Okada A., Yabuki S., Zhang J. and Fan Z. L. (1993) A geochemical study of loess and desert sand in northern China – implications for continental-crust weathering and composition. *Chem. Geol.* **106**, 359–374.

Liu X. Q., Dong H. L., Yang X. D., Herzschuh U., Zhang E. L., Stuut J. B. W. and Wang Y. B. (2009) Late Holocene forcing of the Asian winter and summer monsoon as evidenced by proxy records from the northern Qinghai–Tibetan Plateau. *Earth Planet. Sci. Lett.* **280**, 276–284.

Maher B. A. (2008) Holocene variability of the East Asian summer monsoon from Chinese cave records: a re-assessment. *Holocene* **18**, 861–866.

Marticorena B., Bergametti G., Aumont B., Callot Y., Ndoume C. and Legrand M. (1997) Modeling the atmospheric dust cycle: 2. Simulation of Saharan dust sources. *J. Geophys. Res.: Atmos.* **102**, 4387–4404.

McLennan S. M. (1989) Rare-earth elements in sedimentary-rocks – influence of provenance and sedimentary processes. *Geochem. Mineral. Rare Earth Elem.* **21**, 169–200.

Neff U., Burns S. J., Mangini A., Mudelsee M., Fleitmann D. and Matter A. (2001) Strong coherence between solar variability and the monsoon in Oman between 9 and 6 kyr ago. *Nature* **411**, 290–293.

Nesbitt H. W. and Young G. M. (1982) Early Proterozoic climates and plate motions inferred from major element chemistry of lutites. *Nature* **299**, 715–717.

Nesbitt H. W. and Young G. M. (1996) Petrogenesis of sediments in the absence of chemical weathering: effects of abrasion and sorting on bulk composition and mineralogy. *Sedimentology* **43**, 341–358.

Nesbitt H. W., Young G. M., McLennan S. M. and Keays R. R. (1996) Effects of chemical weathering and sorting on the petrogenesis of siliciclastic sediments, with implications for provenance studies. *J. Geol.* **104**, 525–542.

Osada K., Da H., Kido M., Matsunaga K. and Iwasaka Y. (2004) Mineral dust layers in snow at Mount Tateyama, Central Japan: formation processes and characteristics. *Tellus Ser. B: Chem. Phys. Meteorol.* **56**, 382–392.

Pease P. P. and Tchakerian V. P. (2002) Composition and sources of sand in the Wahiba Sand Sea, Sultanate of Oman. *Ann. Assoc. Am. Geogr.* **92**, 416–434.

Prospero J. M., Ginoux P., Torres O., Nicholson S. E. and Gill T. E. (2002) Environmental characterization of global sources of atmospheric soil dust identified with the Nimbus 7 Total Ozone Mapping Spectrometer (TOMS) absorbing aerosol product. *Rev. Geophys.* **40**.

Pye K. (1987) *Asian Dust and Dust Deposits*. Academic Press.

Schofield P. F., Knight K. S., Covey-Crump S. J., Cressey G. and Stretton I. C. (2002) Accurate quantification of the modal mineralogy of rocks when image analysis is difficult. *Mineral. Mag.* **66**, 189–200.

Steffensen J. P. (1997) The size distribution of microparticles from selected segments of the Greenland Ice Core Project ice core representing different climatic periods. *J. Geophys. Res.: Oceans* **102**, 26755–26763.

Stevens T., Thomas D. S. G., Armitage S. J., Lunn H. R. and Lu H. Y. (2007) Reinterpreting climate proxy records from late Quaternary Chinese loess: a detailed OSL investigation. *Earth Sci. Rev.* **80**, 111–136.

Sun J. M., Zhang M. Y. and Liu T. S. (2001) Spatial and temporal characteristics of dust storms in China and its surrounding regions, 1960–1999: relations to source area and climate. *J. Geophys. Res.: Atmos.* **106**, 10325–10333.

Sun Y. B., Tada R. J., Chen J., Chen H. Z., Toyoda S., Tani A., Isozaki Y., Nagashima K., Hasegawa H. and Ji J. F. (2007) Distinguishing the sources of Asian dust based on electron spin resonance signal intensity and crystallinity of quartz. *Atmos. Environ.* **41**, 8537–8548.

Sun Y. B., Tada R. J., Chen J. C., Liu Q. S., Toyoda S., Tani A., Ji J. F. and Isozaki Y. (2008) Tracing the provenance of fine-grained dust deposited on the central Chinese Loess Plateau. *Geophys. Res. Lett.* **35**, 5.

Svensson A., Biscaye P. E. and Grousset F. E. (2000) Characterization of late glacial continental dust in the Greenland Ice Core Project ice core. *J. Geophys. Res.: Atmos.* **105**, 4637–4656.

Taylor S. R., McLennan S. M. and McCulloch M. T. (1983) Geochemistry of loess, continental crustal composition and crustal model ages. *Geochim. Cosmochim. Acta* **47**, 1897–1905.

Taylor S. R. and McLennan S. M. (1985) *Continental Crust: Its Composition and Evolution. An Examination of the Geochemical Record Preserved in Sedimentary Rocks*. Blackwell Scientific Publications.

Wang P. X., Clemens S., Beaufort L., Braconnot P., Ganssen G., Jian Z. M., Kershaw P. and Sarnthein M. (2005a) Evolution and variability of the Asian monsoon system: state of the art and outstanding issues. *Quatern. Sci. Rev.* **24**, 595–629.

Wang Y. J., Cheng H., Edwards R. L., He Y. Q., Kong X. G., An Z. S., Wu J. Y., Kelly M. J., Dykoski C. A. and Li X. D. (2005b) The Holocene Asian monsoon: links to solar changes and North Atlantic climate. *Science* **308**, 854–857.

Weiss D., Shotyk W., Kramers J. D. and Gloor M. (1999) Sphagnum mosses as archives of recent and past atmospheric lead deposition in Switzerland. *Atmos. Environ.* **33**, 3751–3763.

Wu G. J., Zhang C. L., Gao S. P., Yao T. D., Tian L. D. and Xia D. S. (2009a) Element composition of dust from a shallow Dunde ice core, Northern China. *Global Planet. Change* **67**, 186–192.

Wu G. J., Xu B. Q., Zhang C. L., Gao S. P. and Yao T. D. (2009b) Geochemistry of dust aerosol over the Eastern Pamirs. *Geochim. Cosmochim. Acta* **73**, 977–989.

Xiao J., Porter S. C., An Z. S., Kumai H. and Yoshikawa S. (1995) Grain-size of quartz as an indicator of winter monsoons strength on the loess plateau of central China during the last 130,000-yr. *Quatern. Res.* **43**, 22–29.

Xiong S. F., Ding Z. L., Zhu Y. J., Zhou R. and Lu H. J. (2010) A similar to 6 Ma chemical weathering history, the grain size dependence of chemical weathering intensity, and its implications for provenance change of the Chinese loess–red clay deposit. *Quatern. Sci. Rev.* **29**, 1911–1922.

Yadav S. and Rajamani V. (2004) Geochemistry of aerosols of northwestern part of India adjoining the Thar Desert. *Geochim. Cosmochim. Acta* **68**, 1975–1988.

Yang S. L., Ding F. and Ding Z. L. (2006) Pleistocene chemical weathering history of Asian arid and semi-arid regions recorded in loess deposits of China and Tajikistan. *Geochim. Cosmochim. Acta* **70**, 1695–1709.

Yang X. P., Liu Y. S., Li C. Z., Song Y. L., Zhu H. P. and Jin X. D. (2007a) Rare earth elements of aeolian deposits in Northern China and their implications for determining the provenance of dust storms in Beijing. *Geomorphology* **87**, 365–377.

Yang X. P., Zhu B. Q. and White P. D. (2007b) Provenance of aeolian sediment in the Taklamakan Desert of western China, inferred from REE and major-elemental data. *Quatern. Int.* **175**, 71–85.

Yokoo Y., Nakano T., Nishikawa M. and Quan H. (2004) Mineralogical variation of Sr–Nd isotopic and elemental compositions in loess and desert sand from the central Loess Plateau in China as a provenance tracer of wet and dry deposition in the northwestern Pacific. *Chem. Geol.* **204**, 45–62.

Yu Z. S., Robinson P. and McGoldrick P. (2001) An evaluation of methods for the chemical decomposition of geological materials for trace element determination using ICP-MS. *Geostand. Newsl.: J. Geostand. Geoanal.* **25**, 199–217.

Zdanowicz C., Hall G., Vaive J., Amelin Y., Percival J., Girard I., Biscaye P. and Bory A. (2006) Asian dustfall in the St. Elias Mountains, Yukon, Canada. *Geochim. Cosmochim. Acta* **70**, 3493–3507.

Zhang D. Z., Iwasaka Y., Shi G. Y., Zang J. Y., Matsuki A. and Trochkine D. (2003a) Mixture state and size of Asian dust particles collected at southwestern Japan in spring 2000. *J. Geophys. Res.: Atmos.* **108**.

Zhang X. Y., Arimoto R. and An Z. S. (1997) Dust emission from Chinese desert sources linked to variations in atmospheric circulation. *J. Geophys. Res.: Atmos.* **102**, 28041–28047.

Zhang X. Y., Gong S. L., Shen Z. X., Mei F. M., Xi X. X., Liu L. C., Zhou Z. J., Wang D., Wang Y. Q. and Cheng Y. (2003b) Characterization of soil dust aerosol in China and its transport and distribution during 2001 ACE-Asia: 1. Network observations. *J. Geophys. Res.* **108**. ACH3-1–13.

Zhang X. Y., Gong S. L., Zhao T. L., Arimoto R., Wang Y. Q. and Zhou Z. J. (2003c) Sources of Asian dust and role of climate change versus desertification in Asian dust emission. *Geophys. Res. Lett.* **30**.

Zhang Q. G., Kang S. C., Kaspari S., Li C. L., Qin D. H., Mayewski P. A. and Hou S. G. (2009) Rare earth elements in an ice core from Mt. Everest: seasonal variations and potential sources. *Atmos. Res.* **94**, 300–312.

Associate editor: Sidney R. Hemming